



HAL
open science

Outfitting next generation displays with optical metasurfaces

Inki Kim, Gwanho Yoon, Jaehyuck Jang, Patrice Genevet, Ki Tae Nam,
Junsuk Rho

► **To cite this version:**

Inki Kim, Gwanho Yoon, Jaehyuck Jang, Patrice Genevet, Ki Tae Nam, et al.. Outfitting next generation displays with optical metasurfaces. ACS photonics, 2018, 5 (10), pp.3876-3895. 10.1021/ac-photonics.8b00809 . hal-03584596

HAL Id: hal-03584596

<https://hal.science/hal-03584596>

Submitted on 22 Feb 2022

HAL is a multi-disciplinary open access archive for the deposit and dissemination of scientific research documents, whether they are published or not. The documents may come from teaching and research institutions in France or abroad, or from public or private research centers.

L'archive ouverte pluridisciplinaire **HAL**, est destinée au dépôt et à la diffusion de documents scientifiques de niveau recherche, publiés ou non, émanant des établissements d'enseignement et de recherche français ou étrangers, des laboratoires publics ou privés.

Outfitting next generation displays with optical metasurfaces

Inki Kim,^{†,♯} Gwanho Yoon,^{†,♯} Jaehyuck Jang,^{‡,♯} Patrice Genevet,[§] Ki Tae Nam,^{||} and Junsuk Rho^{†,‡,⊥,*}

[†]Department of Mechanical Engineering, Pohang University of Science and Technology (POSTECH), Pohang 37673, Republic of Korea

[‡]Department of Chemical Engineering, Pohang University of Science and Technology (POSTECH), Pohang 37673, Republic of Korea

[§]Centre de Recherche sur l'Hétéro-Epitaxie et ses Applications, CNRS, Rue Bernard Gregory, Sophia Antipolis 06560 Valbonne, France

^{||}Department of Materials Science and Engineering, Seoul National University, Seoul 08826, Republic of Korea

[⊥]National Institute of Nanomaterials Technology (NINT), Pohang 37673, Republic of Korea

[♯]These authors contributed equally to this work.

*Corresponding author. E-mail: jsrho@postech.ac.kr

Abstract: Optical metasurface, composed of ultra-thin subwavelength meta-atoms, has enabled flat-optics and corresponding flat optical components such as ultra-thin lenses, color filters and absorbers. Among the plethora of applications currently attracting great interest, next generation display techniques could further benefit from metasurface technology. Thanks to relatively simple mechanisms of amplitude and phase modulation of light by the meta-atoms, many of the recent research achievements in metasurfaces are related to display applications. In this Perspective, we focus on metasurface holograms and colorations for projective and reflective display techniques. First, we briefly introduce the working mechanism of metasurface holograms and colorations, and review state-of-the-art techniques in each field from perspective of materials, functionalities, and fabrication methodologies towards real-life display applications. Finally, we conclude on the potential outcome and outlook on this technology and highlight the key challenges to be solved for next generation display.

Keywords: Optical metamaterials, Metasurfaces, Hologram, Structural color printing, Next generation display

Introduction

Optical metamaterials, which are composed of subwavelength meta-atoms, have revolutionized micro and nanophotonics research. Artificially designed meta-structures not only can exhibit unusual electromagnetic properties, such as negative refraction,^{1,2} super-lensing effect³⁻⁵ and cloaking,⁶⁻⁸ but also boost conventional photonic device performances, such as efficiency of solar cells^{9,10} and functionalities of optical components.¹¹⁻¹³ The practical applications of the optical metamaterials have been considerably accelerated in recent years due to the development of two-dimensional optical metamaterials, also called optical metasurfaces.^{14,15} Compared to tricky and difficult fabrication processes of bulk optical metamaterials, metasurfaces can reduce the burden of fabrication difficulties and more importantly, one could substantially shrink the thickness of photonics devices within the range of the working wavelength. For instance, optical metasurfaces can realize flat lenses for focusing and imaging with broadband and achromatic characteristics in whole visible range.¹⁶⁻¹⁸ Because these kind of optical metasurfaces are suitable for mass productions with state-of-the-art photolithography processes, many practical applications can be considered such as flat optical components and next-generation display equipment.

Growing interests in next-generation display techniques for virtual reality (VR), augmented reality (AR),¹⁹ three-dimensional (3D) displays and reflective displays require novel and functionalized equipment like stereoscopic displays, volumetric displays, structure coloring displays and wearable glasses with such display functions. Stereoscopic displays can exhibit volumetric images by generating two different images, which are captured and perceived differently in left and right eye. Volumetric displays can exploit holographic techniques to generate 3D images in free space using spatial light modulators with computer generated holography. Still, these research fields have been investigated very actively. However, there are lots of hurdles of conventional technologies such as small viewing angle, low image resolution (or severe noise) and bulk device volume. Interestingly, by adjusting the phase and amplitude of light and the resonance characteristics of structures with single unit nanostructure of deep subwavelength scale, optical metasurfaces appear as natural device to overcome the hurdles in the conventional technologies, and have merits such as compactness, miniaturization, integrability into flexible substrate, high-resolution and large viewing angle which are preferable in the next-generation display applications.

In this perspective, we will cover metasurface holograms and color printing applications that can be applied to next-generation display technology. We will briefly introduce the history of the development of metasurfaces and report state-of-the-art techniques in metasurface holography and color printing. At last, key challenges and outlooks towards practical applications of this emerging technology for applications in displays will be suggested. In particular, we will focus on more

technical issues and remaining tasks for real applications from the perspective of practicality such as materials and designs for enhancing device efficiency, multi-functionalities, also large-area fabrication and printable methods for mass-productions.

Metasurface holograms for projective display techniques

Since Dennis Gabor's invention in the late 1940's,²⁰ holography as a technique that can reproduce an original light field reflected or transmitted from objects has attracted great interests, in particular due to its promising applications for 3D displays²¹ and optical data storage.²² Spatial distribution of optical waves can be described by its complex amplitude containing both amplitude and phase information, that perfectly encodes a certain optical wave. Whereas typical photographs can only record squared amplitude distribution of the optical wave itself, holography can replicate complex amplitude distribution previously recorded in an interference pattern. Therefore, theoretically, observers cannot distinguish outgoing optical wave of hologram from that of real objects.

When optical waves propagate in the space, their spatial complex amplitude distribution $U(x, y; z)$ along to the propagation direction can be derived by solving Helmholtz equation, and its solution is

$$U(x, y; z) = \frac{1}{4\pi^2} \iint F[U(x, y; z = 0)] \exp\left(-jk_0 z \sqrt{1 - \frac{k_x^2}{k_0^2} - \frac{k_y^2}{k_0^2}}\right) \exp(-jk_x x - jk_y y) dk_x dk_y$$

where k_x and k_y represent spatial frequencies, and k_0 is the size of the wave vector.²³ $F[\cdot]$ denotes Fourier transformation operator. The above equation allows us to figure out diffraction pattern of a certain optical wave reflected or transmitted from objects. If we apply the paraxial approximation, $k_x^2 + k_y^2 \ll k_0^2$, we have the following Fresnel diffraction formula which is more convenient to utilize:

$$U(x, y; z) = \exp(-jk_0 z) \frac{jk_0}{2\pi z} \iint U(x', y'; z = 0) \exp\left\{\frac{-jk_0}{2z} [(x - x')^2 + (y - y')^2]\right\} dx' dy'$$

where x' and y' represent the local coordinate of the object plane.²³

The early holograms were composed of photoluminescent material that stored the squared amplitude distribution of the light impinging on the film. Recording the interference between an object and the reference light on interfering waves, it is possible to retrieve both amplitude and phase information of the object.²¹ The image of the object can be reconstructed by shining a reconstruction beam, identical to the reference beam, on the interference pattern recorded film. Outgoing optical wave can be decomposed into three parts, among one them represents the original object light. The object beam is spatially separated from the unwanted beams using off-axis recording and reconstruction techniques.²³

Together with the development of spatial light modulators (SLMs), computer-generated hologram (CGH) has attracted numerous attention owing to its convenient image generation and versatile applications. The primary difference between CGH and the early film-based hologram is that the former is composed of digitalized pixels while the latter contains continuous amplitude distribution. Therefore, CGH generates a discretized amplitude or phase distribution. CGH can be realized by SLMs to address either amplitude or phase distribution of incident optical waves. Holograms designed to control the phase distribution only are called phase-only holograms.

The kinoform hologram, as one of the phase-only hologram, can be generated by taking the phase information (imaginary part) of the conventional Fourier hologram. The diffraction efficiency of the kinoform hologram is much higher than other CGH techniques such as detour-phase hologram, but the noise of the reconstructed image is severe. To solve this problem, iterative Fourier transform algorithm (IFTA) is routinely utilized to reduce the noise. This algorithm was proposed by Hirsch et al.,²⁵ and the similar one has been applied to retrieve phase information of the hologram by Gerchberg and Saxton.²⁶ So, this algorithm is also called as Gerchberg-Saxton (GS) algorithm. There are many other techniques to improve the fidelity and compensate the distortion of the reconstructed image. Dammann et al. proposed a method to reduce the noise by laser speckle in the reconstructed image.²⁷ Shen et al. introduced a method to compensate the error of the paraxial condition in the Fresnel diffraction formula.²⁸ As the reconstructed image size becomes larger, the paraxial condition does not work well. Hence, Rayleigh-Sommerfeld (RS) diffraction formula which does not assume paraxial condition should be applied instead of the Fresnel diffraction formula. Similar fast-Fourier-transformation algorithms have been proposed to solve RS diffraction problems.

Metamaterials, whose effective properties are adjustable by designing the appropriate unit cell, have been utilized to create holograms. Walther et al. realized the first metamaterial hologram based on metal-dielectric multilayered fishnet structures.²⁹ By controlling bar widths in the structures, they designed the complex transmission coefficient at an incident wavelength of 714 nm. They also realized wavelength multiplexed holograms based on the same fishnet metamaterial.³⁰ Due to the dispersion of this specific metamaterial, a single metamaterial hologram can generate two different holographic images depending on the incident wavelength of 905 nm and 1385 nm. Larouche et al. demonstrated phase-only hologram based on multilayered infrared metamaterial made of metallic I-beam and rectangular patch shaped gold (Au) elements.³¹ Since the effective refractive index of the metamaterial changes depends on the element shape, phase distribution of the metamaterial can be controlled by arranging such elements at appropriate positions. The above mentioned metamaterials, consist of repeated identical resonant structures also called meta-atom. From the material perspective, the optical properties of these metamaterials can be understood using effective medium theory. The

extreme case where metamaterials become infinitely thin, or relatively thin, compared to the wavelength of operation leads to the realization of metasurfaces, *i.e.* wavelength and sometime subwavelength-thin optical devices composed of single layer of spatially varying individually designed scattering antennas to manipulate light properties within subwavelength propagation distance. In this case, the effective medium theory which was well suited for 3D metamaterials, is not valid anymore and a new method essentially based on the boundary conditions of the electromagnetic fields in the presence of the metasurface have to be considered.³²⁻³⁵ The emergence of metasurface has attracted tremendous interest due to its many advantages such as planar characteristics, easy fabrication and high efficiency.³⁶⁻³⁹

The origin of the concept of metasurface can be attributed to Kock as reported in the seminal work to locally reduce the phase velocity of light using subwavelength metallic patches,⁴⁰ followed by Stork et al.⁴¹ and Farn.⁴² In the two latter papers, the authors realized grating structures with a period smaller than the wavelength of light. Efficient blazed gratings for IR featuring subwavelength elements have been reported also in dielectric materials by Prof. Lalanne and co-workers.⁴³ In 2011, Yu et al. demonstrated linear phase gradient metasurface using metallic V-shaped antennas, connecting the deflection capabilities of the devices with the generalized laws of reflection and refraction.⁴⁴ This work pointed out the possibility of addressing the complex amplitude of scattered wave from the metasurface by designing and arranging the appropriate antennas in a single layer. Ni et al. realized a metasurface hologram at the wavelength of 676 nm based on the complimentary V-shaped antennas made of 30-nm-thick Au thin film.⁴⁵ The V-shaped antennas operate for the linearly polarized light, and the scattered light which contains desired complex amplitude has cross-polarization to the incident light. Although V-shaped antennas have been successfully implemented to fully address the complex amplitude of the scattered field, metallic losses and the fact that they work only in cross-polarization limit their utilization for real applications. The concept of holography have been further utilized to accurately predict the far-field, in amplitude phase and polarization of surface waves scattered by a distribution of grooves disposed following holographic patterns.

Circularly polarized light based on Pancharatnam-Berry (PB) phase makes the metasurface design process much simpler than the case of the linearly polarized light. PB phase is also called as geometric phase because the phase of scattered light depends only on the orientation of the structures. Bomzon et al. experimentally demonstrated the circularly polarized light conversion into an azimuthally polarized light by using space-variant grating.⁴⁶ In metasurfaces, Huang et al. imposed PB phase to design metasurfaces of anomalous refraction⁴⁷ as well as the hologram⁴⁸ working for circularly polarized light. This hologram was designed to generate different images depending on the focal length based on Fresnel holography. They filled each unit cell with identical metallic nanorods rotated one with respect to the other, so that the phase of the cross-polarized scattered light is

determined by twice the rotation angle of element. Assuming that a metallic nanorod acts as dipole antenna, the incident circularly polarized light ($+\sigma$) at small incident and observation angles is scattered field in the farfield according to:

$$\mathbf{E}_{\text{rad}} \approx \frac{c\alpha k^2}{4\sqrt{2}\pi r} e^{ikr} \left[\frac{\cos\theta\cos\varphi + 1}{4} \mathbf{E}_{\mathbf{u}}^{\sigma} + \frac{(\cos\theta + 1)(\cos\varphi + 1)}{8} \mathbf{E}_{\mathbf{u}}^{-\sigma} e^{+i2\delta} \right]$$

$$\mathbf{E}_{\mathbf{u}}^{\pm\sigma} = \cos\varphi\mathbf{e}_x \pm \sigma i\mathbf{e}_y - \sin\varphi\mathbf{e}_z$$

where c is speed of light, α is the dipole moment, k is the wave vector, r is the distance from the dipole, θ is the incident angle, φ is the observation angle, δ is the rotation angle of the dipole.⁴⁷ This formula verifies that the cross-polarized scattered light has the phase variation of 2δ . This simple design rule based on PB phase addressing is more intuitive and way more convenient than playing with the resonance properties of V-shaped antennas. The inconvenient part is that the structure has to be addressed optically with circularly polarized beam and that the resulting phase modulated field is also circularly polarized, in the opposite polarization comparing to the incident field.

1) Highly-efficient metasurface holograms

Hologram efficiency, defined as the optical power ratio of the image to the total incident beam, is one of the most relevant parameters for practical application of metasurface holograms. The above examples including fishnet metamaterials, single-layered Au metasurfaces, and their complimentary structures can be used for hologram applications, but their efficiencies are extremely low. Most of the incident optical power does not contribute to the image formation due to the reflection, absorption, and co-polarization beam. Yifat et al. achieved metasurface hologram efficiency of 40-50% at NIR wavelengths based on the metal-insulator-metal (MIM) structure,⁴⁹ and the drastic advance in the efficiency at visible and NIR wavelengths has been achieved by Zheng et al. based on the similar MIM configuration (Figure 1a).⁵⁰ The intermediate dielectric layer works as a Fabry-Pérot cavity: the electromagnetic field from the top antenna reflects from the bottom metal layer and consistently reinforce the antenna resonance of the nanorods; Depending on design, the cross-polarization reflectance can increase up to 80% in the wavelengths range from 600 nm to 1000 nm. Due to the interband transition of Au, the optical loss below 600 nm is still severe. Using silver (Ag, for which interband transition frequency locates near ultraviolet) instead of Au as structuring material, it is possible to improve the hologram efficiency for visible light.⁵¹ Although MIM configuration has successfully demonstrated highly efficient metasurface holograms, their operation is limited to the reflection mode. In the case of transmission mode, dielectric materials can be used to achieve such high efficiency.

Different to metallic components, high-refractive-index dielectric structures can possess not only

electric dipoles but also effective magnetic dipoles inside leading to strong forward scattering.^{52,53} Arbabi et al. demonstrated various metasurfaces such as holograms and lenses operating at the wavelength of 915 nm based on amorphous silicon (a-Si) (Figure 1b).⁵⁴ By controlling specific configuration of the elliptical posts, polarization multiplexed hologram whose efficiency reaching over 84% have been demonstrated, *i.e.* linearly polarized light in x and y direction incident to the metasurface generates different images at the image plane. Huang et al. also demonstrated metasurface hologram for visible light based on a-Si, but the efficiency drastically drops to 3% due to severe optical loss of a-Si at visible wavelengths.⁵⁵ Hence, new materials with low extinction coefficient in visible wavelengths are necessary to overcome the optical loss.

Low-contrast dielectric materials such as titanium dioxide (TiO_2), silicon nitride (SiN), and gallium nitride (GaN) can be suitable candidates as structuring material for metasurfaces to compensate the optical loss in visible wavelengths.^{56,57} Devlin et al. demonstrated a metasurface hologram of the transmission mode with high efficiency around 80% in visible wavelengths by using TiO_2 (Figure 1c).⁵⁸ Extinction coefficient of such material is almost zero in visible wavelengths. Concerning the fabrication of the latter devices, incredibly smooth and regular side walls have been achieved, limiting the roughness along the nanorods surface, therefore limiting undesired additional scattering from the structure. On the other hand, structure height should become higher than that of high-refractive-index materials to achieve comparable conversion functionality. In addition, atomic layer deposition should be accomplished for a long time to fabricate TiO_2 pillar structures, and this impinges on practical applications.

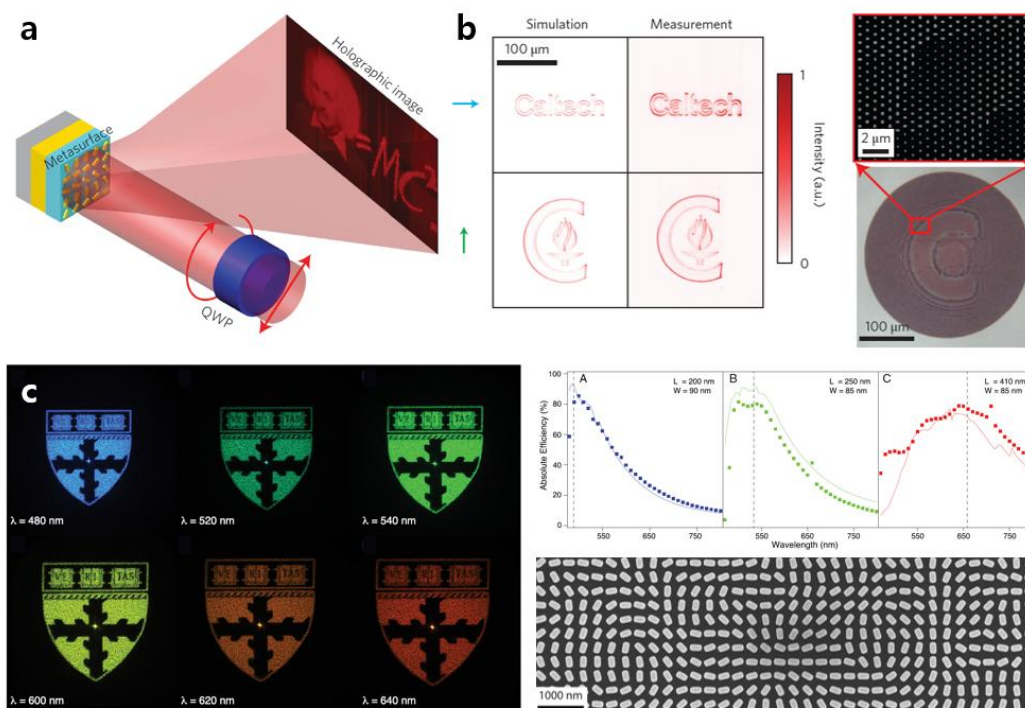


Figure 1. Highly efficient metasurface holograms. (a) MIM based metasurface hologram operating from visible to NIR wavelengths.⁵⁰ The intermediate dielectric layer works as a Fabry-Pérot cavity, so the efficiency reaches 80% in reflection mode. (b) a-Si based metasurface hologram operating at NIR wavelengths.⁵⁴ Due to the strong magnetic dipoles in dielectric structures, hologram efficiency drastically increases up to 84% in transmission mode. (c) TiO₂ based metasurface hologram operating at visible wavelengths.⁵⁸ Extinction coefficient of the material is almost zero in visible region, drastically reducing the intrinsic optical loss of the material, leading to 80% hologram efficiency in transmission mode.

2) Multi-color metasurface holograms

Multi-colored image generation is another critical requirement of metasurface hologram for display applications, increasing the information quantity potentially stored in a single device. Montelongo et al. demonstrated a two-colored hologram operating at the wavelengths of 405 nm and 650 nm based on Ag nanoparticles (Figure 2a).⁵⁹ Two different-sized unit structures that have different half-wave resonance frequencies were employed to generate a binary hologram. In this case, the generated images change according to the incident wavelength. A three-colored metasurface hologram working for linearly polarized light in reflection mode was also introduced by Huang et al. based on aluminum (Al) nanostructures (Figure 2b).⁶⁰ Six kinds of structures which cause same amplitude but 180° different phases for red, green, blue color, respectively, were used as unit cells for a binary hologram. In this type of metasurfaces, each unit cell induces different phase variation for different wavelengths. Li et al. demonstrated PB phase based metasurface hologram of complementary Au nanorods whose unit cells cause identical phase variation regardless of wavelengths (Figure 2c).⁶¹ The device works by generating different images at different focal lengths from one incident light. If we change the incident angle and wavelength, the focal length and color also shift. By using three incident beams with controlling their incident angles, only desired colored images can be focused on the image plane. Wan et al. also demonstrated a similar metasurface hologram made of complementary Ag nanorods for three color hologram.⁶² The amplitude is controlled in two steps, improving the generated image fidelity simply by removing the holes at the positions of the zero amplitude region.

Dielectric materials also can be used for the generation of multi-colored hologram. Wang et al. introduced a PB phase based transmission mode silicon metasurface consisting of three different nanostructures that have different diffraction efficiencies for red, green, blue color, respectively (Figure 2d).⁶³ Each structure has almost zero efficiency for the other two wavelengths. Therefore, in contrast with the aforementioned three-colored holograms which produce undesired images around the image plane, the generated holographic image contains desired three-colored image only. This

concept also can be applied for the reflection mode metasurface hologram.⁶⁴ In this work, origin symmetry of the conjugate image of Fourier holography is exploited to add color changing effect according to the state of the incident polarization.

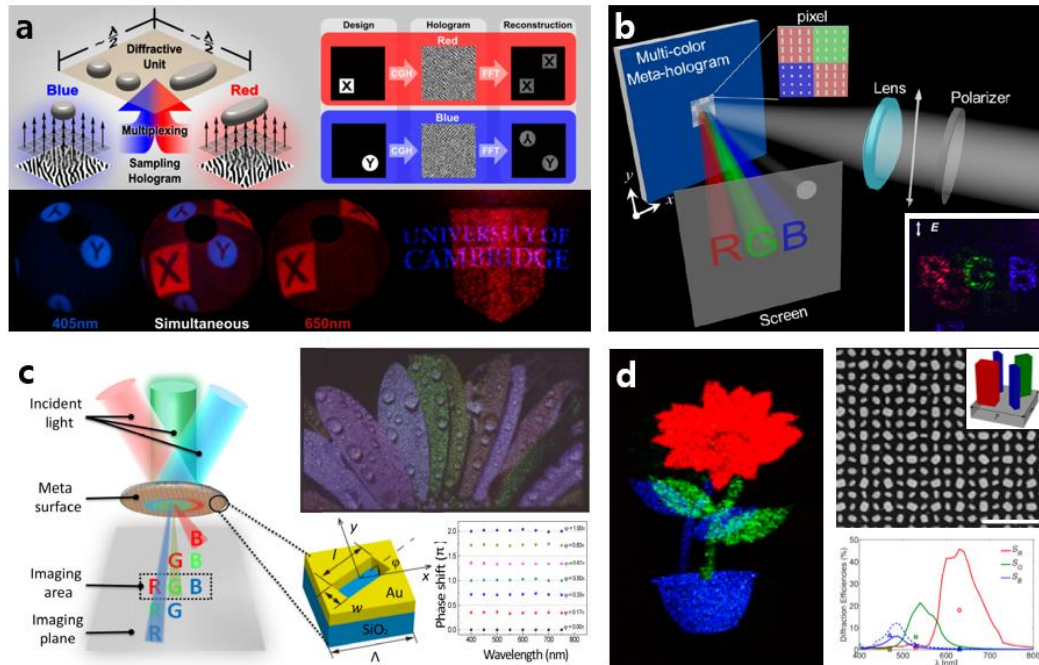


Figure 2. Multi-colored image generation from a single metasurface. (a) Two-colored binary hologram operating at the wavelengths of 405 nm and 650 nm realized by two kinds of Ag nanoparticles with different lengths.⁵⁹ Due to the nature of the binary hologram, conjugate images always appear at the image plane in the origin symmetric form. (b) Three-colored hologram demonstrated from MIM-based metasurface working for linear polarization.⁶⁰ Six kinds of Al nanorods induce same amplitude with out-of-phase variation for red, green, blue, respectively. (c) Complementary Au nanorods generating different images with different focal lengths operating for circular polarization.⁶¹ By controlling the incident angles of each beam, the desired three-colored image can be focused at the intended image plane. (d) a-Si metasurface hologram whose unit cell is multiplexed with three structures.⁶³ Each kind of structure has almost zero diffraction efficiencies except for the target wavelength to enable phase manipulation for three different wavelengths independently.

3) Multi-functionality of metasurface holograms

Multi-functionality is a unique advantage of metasurface hologram compared with conventional holograms generated by SLMs. Since the metasurface manipulates incident light based on scattering rather than simple refractive index control, more degree of freedom in light manipulation are available.

The representative example is multi-image generation by switching the incident polarization. Chen et al. demonstrated MIM-based reflective metasurface hologram that produces different images with polarization directions of incident linearly polarized light (Figure 3a).⁶⁵ Cross-shaped antennas, equivalent to two nanorods oriented perpendicular to each other, can exhibit different resonance characteristics as well as reflection phase variation for linear polarization aligned with their two axes. Montelongo et al. have demonstrated similar holograms based on orthogonally oriented plasmonic nanorods at visible wavelengths.⁶⁶ The last two examples share the same polarization sensitive phase addressing mechanism, *i.e.* the fact that resonance characteristic of a single rod excited by a linear polarization aligned with its axis is much sensitive to the longitudinal length rather than the transverse length.

Multi-image generation from metasurface excited by circularly polarized light is also possible. Huang et al. demonstrated a metasurface hologram that can generate different images with different incident polarizations.⁶⁷ Based on Fresnel holography, they have encoded multiple images located back and forth of the metasurface. If we change the incident circular polarization state from right-hand (RCP) to left-hand (LCP), phase gradient of the metasurface is reversed resulting image position change, *i.e.* images in front space of the metasurface move to back space of the metasurface and vice versa. Therefore, if we focus a fixed image plane, it seems that the image can be changed as the incident polarization changes. Completely independent phase control of arbitrary orthogonal states of polarization is introduced by Mueller et al. by controlling both the orientation (geometric phase) and size (propagation phase) of nanorods (Figure 3b).⁶⁸ They also demonstrated a Fourier-type metasurface hologram which can produce two different images with RCP and LCP, respectively. Another way to generate multi-image for circular polarization is to combine geometric phase with detour phase. Khorasaninejad et al. demonstrated such metasurface based on TiO_2 as structuring material.⁶⁹ Since the addition of the detour phase provides additional degree of freedom for the manipulation of the phase response, it was possible to realize different images with RCP and LCP.

Multi-functionality of the metasurface is not limited to the polarization switching. Kamali et al. demonstrated a new type of multi-functional metasurface which can generate different images with different incident angles by tailoring angular response of U-shaped dielectric antennas (Figure 3c).⁷⁰ Compared with conventional thin diffractive elements whose angular response is highly correlated, this metasurface breaks the angular correlation enabling independent phase masks encoding into a single device. Nonlinear response of metallic antennas also can be used for the multi-functionality.⁷¹ Ye et al. introduced rotating split-ring resonators (SRRs) produce not only cross-polarization beam of the fundamental frequency with $2\sigma\varphi$ phase, but also co- and cross-polarization of the second harmonic frequency with $\sigma\varphi$ and $3\sigma\varphi$ phase, respectively (Figure 3d).⁷² By judiciously arranging the metallic SRRs, they realized three different images depending on the polarizations and frequencies. Third

harmonic generation based on V-shaped metallic antennas also can be used in the nonlinear regime yielding to the same application.⁷³

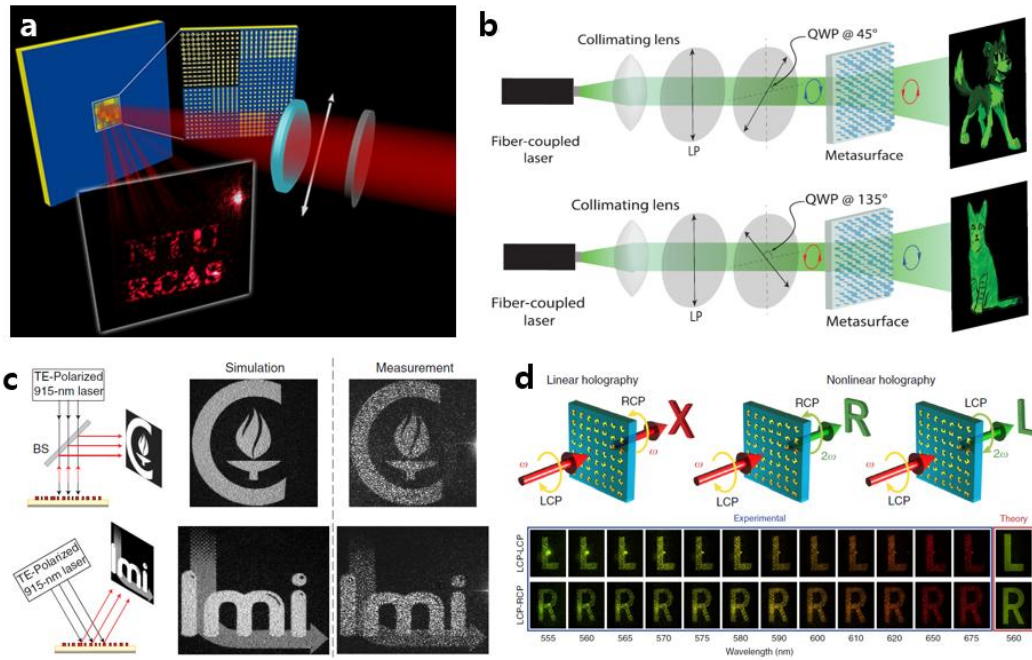


Figure 3. Multi-functional metasurface holograms. (a) Independent control of image generation in the MIM metasurface by switching the polarization direction of linearly polarized light.⁶⁵ Cross-shaped antennas allow us to independently control the resonance characteristics of orthogonally polarized light by adjusting each arm length. (b) Combination of the geometric phase and propagation phase for the independent phase control of arbitrary orthogonal states of polarization.⁶⁸ (c) The angle-multiplexed metasurface hologram.⁷⁰ By tailoring the angular response of U-shaped dielectric antennas, the angular correlation can be broken enabling independent phase mask encoding. (d) The nonlinear metasurface consists of SRRs which produce second harmonic generation with different phase variation in addition to the fundamental frequency.⁷² Three different images can be generated depending on polarization and wavelengths.

In contrast to the previous discussion on polarization-dependent phased array devices, removing the polarization dependence can be useful for practical applications, simplifying the operational scheme. Since the study on directional scattering and associated phase of silicon nanodisks, *i.e.* element without form birefringent property, by Staude et al.,⁴⁶ many related works have been reported including holograms based on a-Si.⁷⁴⁻⁷⁶ Their design principle relies on assembling along the interface array of circularly symmetric nanoposts or nanopillar structures with different radii corresponding to specific phase values. Although a-Si is feasible material for metasurface holograms in NIR

wavelengths, visible wavelengths cannot be covered due to its severe optical loss. Yoon et al. demonstrated polycrystalline silicon (poly-Si) based metasurface hologram at the wavelength of 532 nm, achieving higher efficiency than with a-Si.⁷⁷ Another type of polarization independent metasurface hologram is demonstrated by Huang et al. based on nanoholes on the Au thin film.⁷⁸ Different to the aforementioned examples dielectric circular posts, each nanohole has an identical size and acts as a point source of the Huygens-Fresnel principle. The hologram can be realized by arranging the nanoholes in appropriate positions.

Although various kinds of metasurface holograms have been demonstrated, most of them belong to the phase-only holograms and cannot provide real three-dimensional perspective of objects. To perfectly mimic the object light, spatial phase distribution control should coincide with spatial amplitude distribution control. Xie et al. demonstrated a metasurface hologram working for linearly polarized light based on the detour phase to manipulate the complex amplitude distribution.⁷⁹ The unit cell consists of perpendicularly oriented slits on Al thin film. The position of the slits determines the detour phase while their number affects the transmission amplitude of the unit cell. Lee et al. introduced X-shaped antennas made of poly-Si that can support broadband complex amplitude control for circularly polarized light in visible wavelengths.⁸⁰ In this case, the rotation angles of the antennas are related to the phase variation while the included angles between two sub-rods are associated with the amplitude variation. Thus, this complex amplitude manipulation from the X-shaped antennas could reduce the noise of Fresnel holograms compared with typical phase-only metasurface holograms.

Relying on similar PB holographic metasurfaces concept, a new type of holographic interface, which is able to manipulate the three fundamental properties of light (phase, amplitude, and polarization) over a broad wavelength range has been proposed. The design strategy relies on replacing the large openings of conventional holograms by arrays of subwavelength apertures, oriented to locally select a particular state of polarization. The resulting optical element can therefore be viewed as the superposition of two independent structures with very different length scales, that is, a hologram with each of its apertures filled with nanoscale openings to only transmit a desired state of polarization. These features extend the functionality of conventional printable wavelength-scale binary holograms, which can manipulate complex scalar fields, to include control of the polarization of light.

In addition, several inspirational works on metasurface holograms have been reported. Li et al. demonstrated dual-magnetic resonance based a-Si metasurface holograms whose building blocks have only quarter-wavelength thickness.⁸¹ Conventional dielectric metasurfaces usually need higher thickness of building blocks than metallic metasurfaces based on MIM structures. Reducing the thickness can be beneficial for practical lightweight applications. Liu et al. proposed metasurface holograms relying on the concept of ghost imaging for encryption and security.⁸² They combined a

random binary mask on the metasurface hologram to encrypt the holographic image, and showed that one can obtain the original image by correlation calculations. Malek et al. demonstrated a tunable metasurface hologram utilizing flexible polydimethylsiloxane (PDMS) substrate.⁸³ The metallic metasurface which was encoded by a three-dimensional phase-only Fresnel hologram of multiple images was defined on the PDMS substrate. If the device is stretched, focal lengths of encoded images change; changing the image on the fixed image plane.

Metasurface colorations for reflective display techniques

Structure coloring based reflective display has recently been proposed as the next-generation display technology, generating colors using external light sources. Reflective displays composed of functionalized layers generally reflect RGB colors from external light sources which reduces power consumption.⁸⁴ Because of its distinctive features, the reflective display, which is regarded as echo-display, can be considered as electronic paper (e-paper) and for foldable display applications (a typical example product includes Kindle Paperwhite E-reader by Amazon,⁸⁵ interferometric modulator display (IMOD) by Qualcomm and Electro-Wetting display by Liquavista). However, reflective display technology still has obstacles for practical uses such as brightness/contrast control, vivid and various color generation. Research progress on structure-based coloration reported so far includes photonic crystals,⁸⁶⁻⁸⁸ colloidal nanoparticles,^{89,90} metallic and dielectric gratings,⁹¹⁻⁹⁵ multilayer thin film^{96,97} and metasurfaces.

Metasurfaces coloration techniques, or nanostructure induced coloration, have been investigated intensively due to its advantages on higher spatial resolution, viewing angle independence and lasting durability compared to conventional pigment oriented and other structure based color generation techniques.^{98,99} While applications of metasurfaces for holography are mainly concerned with phase modulations of transmitted or reflected light, color applications requires modulation of amplitude of incident light by nanostructures. Research on metasurface based color printing started by the exploitation of the plasmonic response of metallic nanostructures. The scattering of light using locally excited surfaces plasmons (or collective oscillation of electrons) enable a color printing technique with ultrahigh resolution of ~100,000 dots per inch (dpi), comparable to the diffraction limit of light.¹⁰⁰ Many different of metallic geometries such as nanorod,¹⁰¹⁻¹⁰³ nanoholes,¹⁰⁴⁻¹¹² gratings¹¹³⁻¹¹⁵ and metal-insulator-metal (MIM)¹¹⁶⁻¹²⁰ have been suggested and depending on the excited surface plasmon modes (or geometric resonances) on those structures, generated colors have different characteristics. In terms of materials, noble metals like Au and Ag have typically been used in plasmonic colors and according to their resonance characteristics in visible light, performances of color vibrancy, brightness and contrast vary. However, large interband absorption occur at higher

frequency of visible light such as blue and purple range, which is detrimental for broadband coloring application as it deteriorates color saturation.

An alternative approach to circumvent the optical loss in plasmonic colors, new efforts on all-dielectric based coloring surfaces have been investigated. High index dielectric materials can confine electric and magnetic multipoles in sub-wavelength volumes, the so called Mie resonances of dielectric particles, which can be controlled to generate different colors. a-Si,¹²¹⁻¹²³ crystalline silicon (c-Si),^{124,125} silicon based composition¹²⁶⁻¹²⁷ and titanium oxide^{128,129} based color generation were reported. For the case of silicon metasurfaces, due to high refractive index, the electric and magnetic dipoles of nanoparticles stand in visible range, exhibiting diffusion of light with distinct colors. The advantage of dielectric nanostructuring with respect to plasmonic based interfaces is two folds: 1) dielectrics have low-loss characteristics in visible and 2) Their fabrication process is compatible with metal-oxide-semiconductor (CMOS) fabrications, which is also important consideration for mass production. With the development of dielectric metasurface color printing technology, the technology is becoming more and more suitable for applications on reflective displays. Particularly, recent researches on metasurfaces based color printing have been focused on highly vibrant and vivid color generation, dynamic tunability and high-throughput, large scale fabrication method towards real-life application. Relying on recently published papers, we will cover these issues and offer an outlook, perspectives and challenges for practical metasurfaces based display technology.

1) Highly vibrant and broad structural color generation

Highly saturated and vibrant color spectrum are ones of the most crucial factors in display technology. Among the plasmonic color researches, MIM structure is outstanding candidate for the distinct coloration.¹¹⁶⁻¹²⁰ To achieve vibrant reflective color, resonance with high Q factor should be achieved. Sharp resonance condition with high Q were observed in silver-aluminium oxide-silver (Ag-Al₂O₃-Ag) using hybridization between Wood's anomaly and in-phase electric dipole mode (Figure 4a).¹²⁰ This hybridization enables stronger light confinement in MIM tandem nanodisk than in single Ag structure.

As discussed briefly, unavoidable plasmonic loss in visible regime can be circumvented using lossless high index all-dielectric nanoresonators such as all-dielectric antenna composed of silicon in various state, silicon with antireflection layer, titanium oxide, silicon based composite. The nano-dielectric antenna is capable of reflecting and transmitting light at specific wavelength in the visible depending its geometry and optical properties. Selective directional scattering can be obtained by manipulating both electric and magnetic dipole in specific regimes as suggested by Kerker¹³⁰. The dominant forward and backward scattering of the dielectric nanoparticle array enables greatly

selective reflection/transmission at certain wavelengths, which becomes important to achieving highly-saturated colors. For instant, single color source using Mie resonance of high refractive index silicon nanostructures have been demonstrated,¹³¹⁻¹³³ which enables unprecedented high dpi far beyond conventional display (Figure 4b).¹²¹ However, high extinction coefficient of silicon in blue region and leaky modes from substrate prohibit the realization of saturated colors. Leakage in the substrate can be circumvented by depositing index-matching anti-reflection (AR) coatings.¹²³ This AR coating can be designed to mimic free space impedance, and therefore restoring the matching conditions for unidirectional scattering conditions as suggested by Kerker (Figure 4c).

Many attempts to replace silicon and enhance color quality have been explored with silicon-composite and other dielectric material such as TiO₂. TiO₂ metasurfaces has been regarded as a candidate for all-dielectric coloration due to near-zero extinction coefficient in overall visible, especially in short wavelengths.^{128,129} TiO₂ array plays a role as 2D photonic crystal, which form photonic bandgap according to their lattice constant. The photonic bandgap by TiO₂ scatterers enables highly selective reflection of light for vibrant and saturated color (Figure 4d). By controlling lattice constant and the geometry of the scatterer, the coupling effect between photonic crystal radiation and Mie-resonances will enhance reflectance and sharp resonance with high Q factor. Even though the latter TiO₂ metasurface leverage on collective scattering effects which limits the maximum dpi, the color brightness and the large color gamut make this approach potentially interesting for display applications.

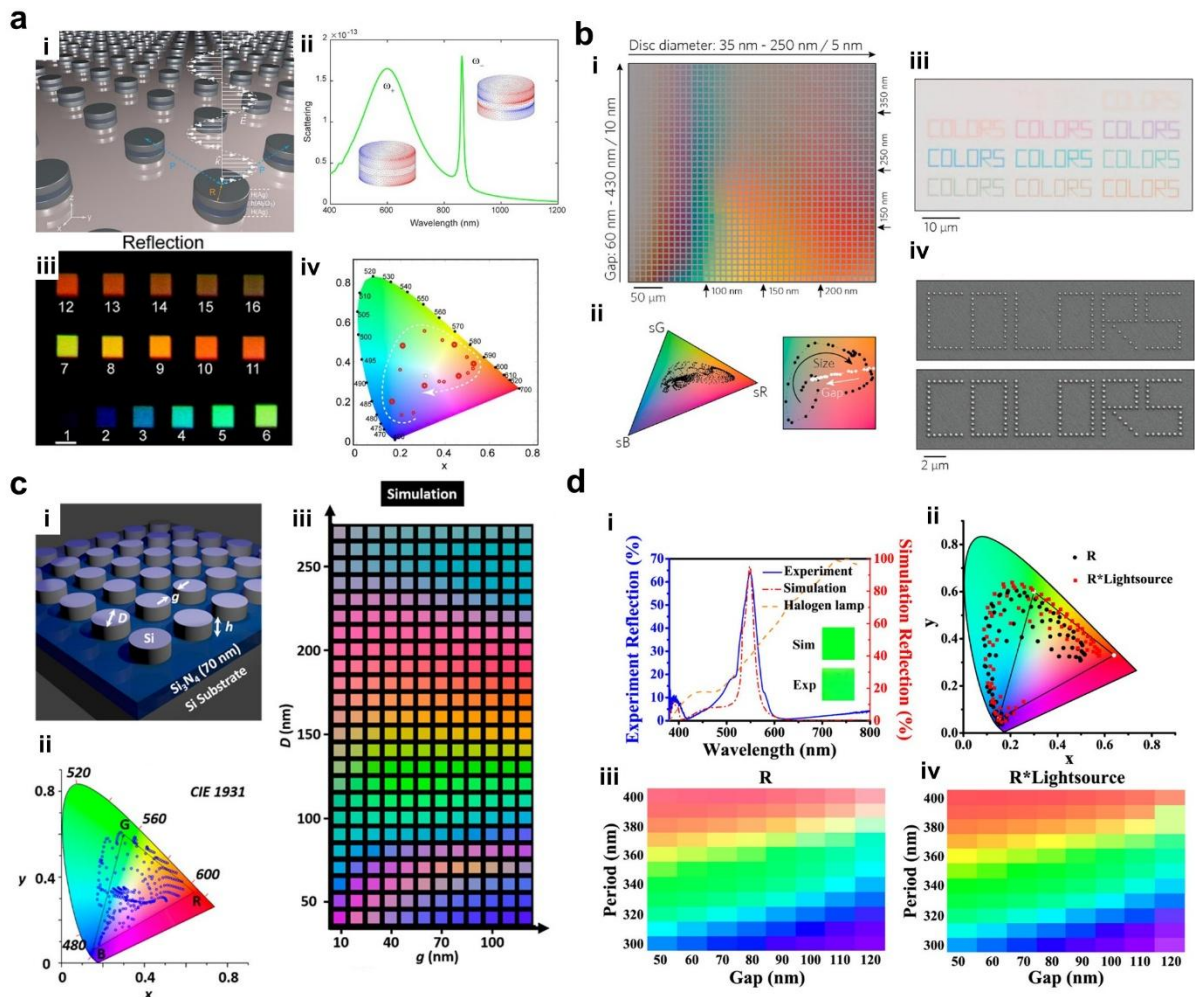


Figure 4. A variety of vibrant and broad structural colors. (a) (i) schematic of plasmonic structural color using Ag-Al₂O₃-Ag nanodisks. (ii) Scattering cross-section of in-phase and out-phase resonance mode. (iii) Color palette and (iv) color gamut of MIM tandem nanodisks.¹²⁰ (b) a-Si based structural color. (i) color palette with disc diameter (x-axis) and gap distance (y-axis). (ii) sRGB colorspace of the experimental result with changing disc diameter and gap. (iii) ‘COLORS’ text printed by single silicon Mie-scatterer and (iv) its SEM image.¹²¹ (c) Silicon nanostructures with anti-reflection coating to mimic free-space environment. (i) color gamut and (ii) color palettes.¹²³ (d) TiO₂ metasurface for full-color printing. (i) Reflection spectrum displaying high Q resonance. (ii) color gamut with directly calculated (black dot) and corrected (red dot) design. Color palette in case of (iii) direct calculation and (iv) corrected calculation considering light source spectrum.¹²⁸

2) Dynamic and tunable structural color

The metasurface coloration techniques have inherent limitation as reflective display applications,

simply because of the static color rendering. After designing and fabricating the structures, their color responses cannot be tuned. Recently, people have started to exploring dynamic and tunable color mechanisms in metasurfaces through mechanical deformation,¹³⁴⁻¹³⁷ liquid crystal,¹³⁸⁻¹⁴⁰ electric stimulus,¹⁴¹⁻¹⁴³ chemical reaction,¹⁴⁴⁻¹⁴⁷ polarization dependence,^{101,111,112,113-115,118,125,148,149} and insulator-metal transition.¹⁵⁰

2-1) mechanical deformation

Stretchable plasmonics with elastomeric substrate enables mechanically tunable structural colors.¹³⁷ Halas et al. designed tunable plasmonic nanostructures composed of two-dimensional periodic array of rectangular Al patterns. When the periodic array is in its relaxed state (Figure 5a), the color rendering is bright green. Under gentle elastic modulation along horizontal axis the lateral space between neighboring particle is increased, which induces red-shifting of the scattering spectrum. On the other hand, when stretched along vertical axis, the interparticle distance is shorten in horizontal axis, blue-shifting the resonance peaks. As a result, this two dimensional stretching mechanism yields highly vivid and broad plasmonic color tuning. This technology can be integrated into micro-electromechanical system (MEMS) such as MEMS-based spectrometers and dynamic color filters.

2-2) Liquid crystal

Liquid crystals (LC) are essential key-elements to connect planar optics with conventional electrically-driving technologies. LC has topological anisotropy and rearrange under voltage bias over threshold (the so called Fréedericksz transition) to filter linearly polarized light. This rearrangement mechanism has been utilized for conventional liquid crystal display (LCD). Accordingly, LCs can act as an effective-index-tunable medium and can be combined with metasurface coloration^{138,139} or polymeric polarizer filter^{140,151} for tunable structural colors. Park et al. assembles LCs as a polarization filter in cells that contain two-dimensional aluminum grating and additional polarization filters.¹⁵¹ With no voltage applied, the linear polarization of input beam is rotated 90°. Under sufficiently large voltage appliance V_0 , the polarization is preserved due to perfect rearrangement of LCs. Thus, the two polarization states coexist when applied voltage over threshold and less than V_0 . Moreover, the mixing ratio of the polarizations can be manipulated by adjusting applied voltage, and the output colors determined by mixture of two primary colors from grating optical responses in two orthogonal polarization states can be electrically and dynamically tuned. On the other hand, the mechanisms utilizing the tunable effective-index property of the LCs medium is different than simply introducing tunable phase delay between two states of polarization during light propagation in the cell.^{138,139} LCs layer on plasmonic metasurfaces instead are varying the dielectric constant of the medium surrounding the antennas, thus influencing their spectral responses, resulting in different colors. Chanda et al.¹³⁹ have reported dynamic coloring through the applied electric field and have been able to integrate plasmonic colors with existing LCD technology with thin-film-transistor array (Figure 5c).

They achieved rather small tunable color spectrum; nevertheless, the combination of plasmonic colors with electrically-driven device pave a substantial way towards real-life applications of structural color.

2-3) Chemical reaction

Liu et al.¹⁴⁵ explored a dynamic plasmonic display using unique hydrogenation/dehydrogenation mechanism of magnesium (Mg) nanoparticles. This chemical mechanism accompanies metal-to-dielectric phase transition of Mg nanoparticles to magnesium hydride (MgH₂). Exposing palladium (Pd) capping layer to a hydrogen (H₂) gas, dissociation of hydrogen molecules into hydrogen atom favors the diffusion into the Mg layer. The Mg nanoparticles absorb H₂, and lose their metallic characteristics. This absorption in response to H₂ is reversible; after dehydrogenation, Mg recovers its plasmonic features. As a demonstration, the vivid-colored images are erased under H₂ exposure and can be restored with oxygen loading (Figure 5b).

Chu et al.¹⁴⁷ suggest bimetallic nanodots arrays with electrochemical bias for real-time dynamic color modulation. During electro-deposition process, Ag shell is being formed on Au nanodome-electrode, inducing red shift of resonance peak. Electro-stripping process, on the other hand, makes reversible reaction with blue shift of resonance. Those reciprocal processes present an obvious redox reaction of Ag, which enable reconfigurable structural plasmonic colors. They demonstrate biomimetic active camouflage with plasmonic chameleon (Figure 5d). The chameleon is covered with fish-scale-like plasmonic color pixel. Color sensors installed inside the chameleon obtain chromatic information from outside. The information is analyzed and delivered to individual patches, tuning their color accordingly.

2-4) Polarization

1-D^{91,93,95} and asymmetric 2-D^{111,112} gratings have different optical responses with respect to horizontally- and vertically-polarized light. This birefringence response can be utilized for tunable color mechanism. Takahara et al.¹²⁵ proposed all-dielectric structural colors by two-dimensional grating composed of c-Si optical antennas (Figure 5e). Asymmetric rectangular structure possesses polarization-dependent properties so that single pixel can display two distinct colors under horizontal and vertical polarization states. Besides, the individual c-Si antenna supports Mie-resonance that generates single color pixel offering high spatial resolution down to the diffraction limit. However, the color tunability requires manual control of a polarizer or a waveplate inserted between the light source and the metasurface. Innovative methods to combine switch between these two states of form birefringence response using external stimulus are required. As mentioned in LCs section, the polarization is well-controlled using LC technology and electrically-driven device.^{140,151} Especially, all-dielectric and highly-asymmetric structural color compatible with LC layer is promising for large and broad tunable color printing.

2-5) Phase-change materials

So far, numerous efforts for tunable material properties have been devoted to transparent conducting oxide as well as phase-transition materials for tunable nanophotonic devices. Phase-change material, one of the tunable materials, changes its state from metal to insulator or vice versa through a change of external parameters such as temperature. This reconfigurable mechanism is realized in vanadium oxide (VO_2), which undergoes insulator-metal transition around 68°C . The transition accompanies dynamic change of electric and optical property, and therefore VO_2 can be used for tunable and real-time structural color. Wang et al. combined VO_2 with plasmonic nanostructures to generate tunable colors.¹⁵⁰ This nanostructure consists of Ag nanodisks as top layer, VO_2 film as bottom, and a silicon dioxide film sandwiched between them. As temperature increases, phase-transition of VO_2 film occurs accompanying change of its optical properties such as real and imaginary part of refractive index. This temperature-dependence phase change enables tunable and reconfigurable color. Pioneering work related to the tunable plasmonic antennas by taking advantage of the thermally driven insulator to metal transition in VO_2 were demonstrated at mid-infrared frequencies¹⁵².

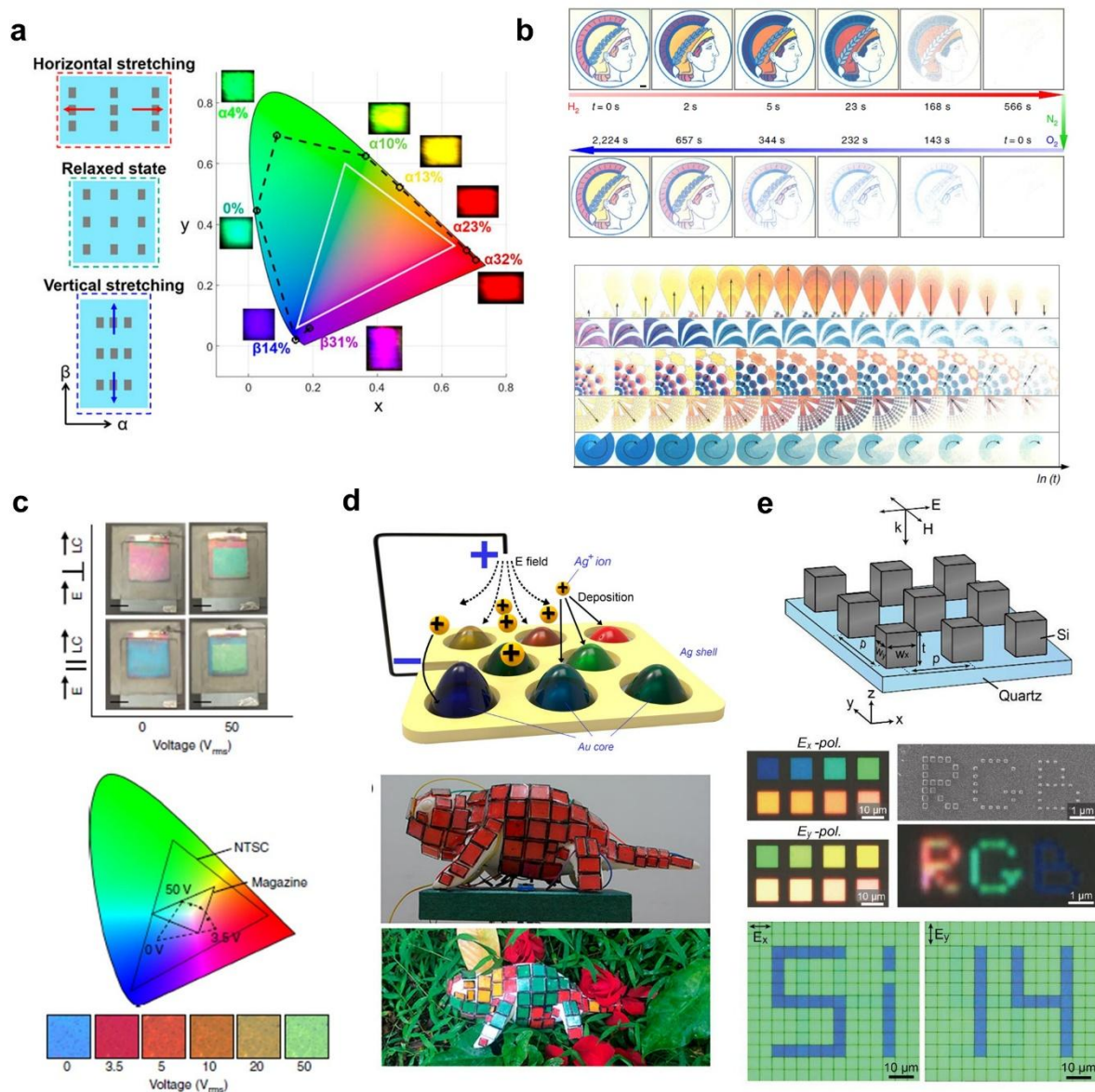


Figure 5. Various types of tunable structural color printing. (a) Mechanically-deformed structural color. Horizontally applied strain induces red-shifted spectrum and vertically applied strain induces blue-shifted spectrum.¹³⁷ (b) Max-Planck-Society's Minerva logo, firework color writing and erasing using hydrogenation and dehydrogenation of MIM structure.¹⁴⁵ (c) Nano-well-structure combined with LC whose orientation is rearranged by applying electric field. Voltage bias enables dynamic color change.¹³⁸ (d) Schematic of real-time color tuning with electro-deposition, stripping controlled by voltage bias and its camouflage application.¹⁴⁷ (e) Rectangular shaped c-Si metasurfaces. Optical responses under x- and y-polarization differ from each other due to asymmetric unit structures.¹²⁵

3) Large-area fabrications and applications

Techniques to address and enhance the scattering of light with metasurfaces have been developed along with the development in nanofabrication techniques. As the coloration properties are mainly determined by the metasurfaces geometry, the influence of nanopatterning techniques for multi-dimensional fabrication and arbitrary shape patterning are critical. In terms of the requirements, electron beam lithography (EBL) process is the one of the most typical nanopatterning tools. By electron beam scanning, EBL can produce ultra-fine nanostructures with multi-dimensional and arbitrary shapes, required for addressing various colors on demand. However, considering fabrication time, cost and device area, the serial scanning type EBL is not the most suitable and optimal method. The writing process, including electron backscattering and charging effects, restricts the type of substrates.

Recently, as an alternative to EBL process, many scalable nanofabrication techniques have been introduced in metasurface coloration from the traditional manufacturing technologies to current state-of-the-art nanofabrications. For instance, imprinting,¹⁵³⁻¹⁵⁵ molding¹⁵³ and roll-to-roll printing technique,¹⁵⁴ which enable centimeter scale or meter scale fabrications, are adopted to print nanoscale structures on rigid or flexible substrates. Also laser interference lithography (LIL),¹⁵⁶ laser printing using laser-matter interactions¹⁵⁷⁻¹⁵⁹ and bottom-up self-assembly fabrications have been reported.¹⁶⁰⁻¹⁶⁴ While these techniques do not yet completely control the dimensions, shapes and materials of metasurfaces, they have allowed metasurface coloration techniques to be closer to commercialization.

Nanoimprinting and molding approaches are straightforward method to print nanoscale patterns in large-area with lithographically patterned rigid mold. Even though one has to fabricate nanoscale mold using EBL or photolithography process in advance, once the mold is fabricated, it can be used repeatedly. Figure 6a shows schematic for polymer replication (or hot embossing) based fabrication using rigid silicon mold.¹⁵³ Lithographically defined silicon molds are used to extrude nanoscale patterns on polymer, followed by Al layer deposition on top, MIM type plasmonic configuration have been realized. The printed metasurfaces image present identical colors independent of the viewing-angle. (Figure 6b) Furthermore, one can use the rigid mold in a roll-to-roll printing system and film insert molding to fabricate metasurfaces in large-areas, as shown in Figure 6c.¹⁵⁴ These kinds of traditional manufacturing techniques will enable metasurfaces printing on arbitrary substrates. (Figure 6d)

LIL is well-known large-area fabrication tool that could fabricate metasurfaces on centimeter scale area or more. However, as it exploits interference characteristic of light, it only makes periodic nanostructures with fixed geometries like lines, circles and holes over the whole exposed area. In the linear regime of photoresist exposition, the feature sizes are also limited by the diffraction limit. Thus, it is hard to display different kinds of subwavelength scale color pixels using LIL.¹⁵⁶ The way to produce subwavelength color pixels using lasers is laser printing techniques. By exploiting photo-

thermal effects during light-matter interaction with the nanostructures, their morphology can be tuned and various colors can be achieved.¹⁵⁶⁻¹⁵⁸ The laser printing technique can be applied for both metallic and dielectric nanostructures, and especially for metallic structures plasmon-assisted photo-thermal effects occur as metallic nanostructures melt easily. On the other hand, dielectric nanostructures strongly absorb the incident light at resonances and the morphology of spatially localized nanostructures can be deformed. Figure 6e and 6f show laser color printing techniques using metallic^{156,159} and dielectric nanostructures,¹⁵⁸ and represent demonstrated printed colorful images from high-index dielectrics. First, polymer replication is used to extrude nanopillar structures and metallic (Al) and dielectric (Ge) layers are deposited respectively. After that, by irradiating laser with different energy density, morphology of nanostructures is tuned, exhibiting different colors. Thus, subwavelength pixels can be fabricated within few ns and as the laser printing exploits localized photo-thermal heating, the pixels can be printed on flexible substrates in large-area.

Bottom-up fabrication methods also can be applied in large-area fabrications for color printings. For instance, self-assembled colloidal nanoparticles can be used as an etching mask or patterning mask for large-area nanopatterning. By changing diameter of particles, pitch between the particles and nanostructure geometries (thickness or shape), displayed colors can be tuned (Figure 7a).¹⁶¹ In addition, self-assembled colloidal nanoparticles can be used as color pixels themselves with top-down lithographic techniques. Nanoparticles on metal-thin insulator films have gap distinct plasmon mode and thus by changing the particle size and gap size, different colors can be realized. Cluster of nanoparticles of different size are designed and patterned to absorb red, blue and green colors. By varying number of particles of each color (or patterned area) one can mix their response to create different colors. Colorful images composed of different color pixels can then be realized with assistance of programmable photomasks and conventional UV lithography process (Figure 7b).¹⁶³ Furthermore, recently functional chiral nanoparticles have been reported and they suggest soft metamaterials based bulk color filters in an economical way.¹⁶⁵ Unlike reported conventional achiral nanoparticles, the self-assembled plasmonic chiral particles can exhibit different absorption of light depending on their different state of circular polarizations (Figure 7c). These chiral particles can also rotate visible light due to optical rotatory dispersion response. Simple color modulation system in a bulk system is demonstrated using a set of polarizers. By varying angle of polarizers one can modulate light intensity and tune the transmitted colors. These kinds of hybrid approaches combining top-down and bottom-up based fabrications can pave the way towards cost-effective, large-area and vibrant color printing techniques.

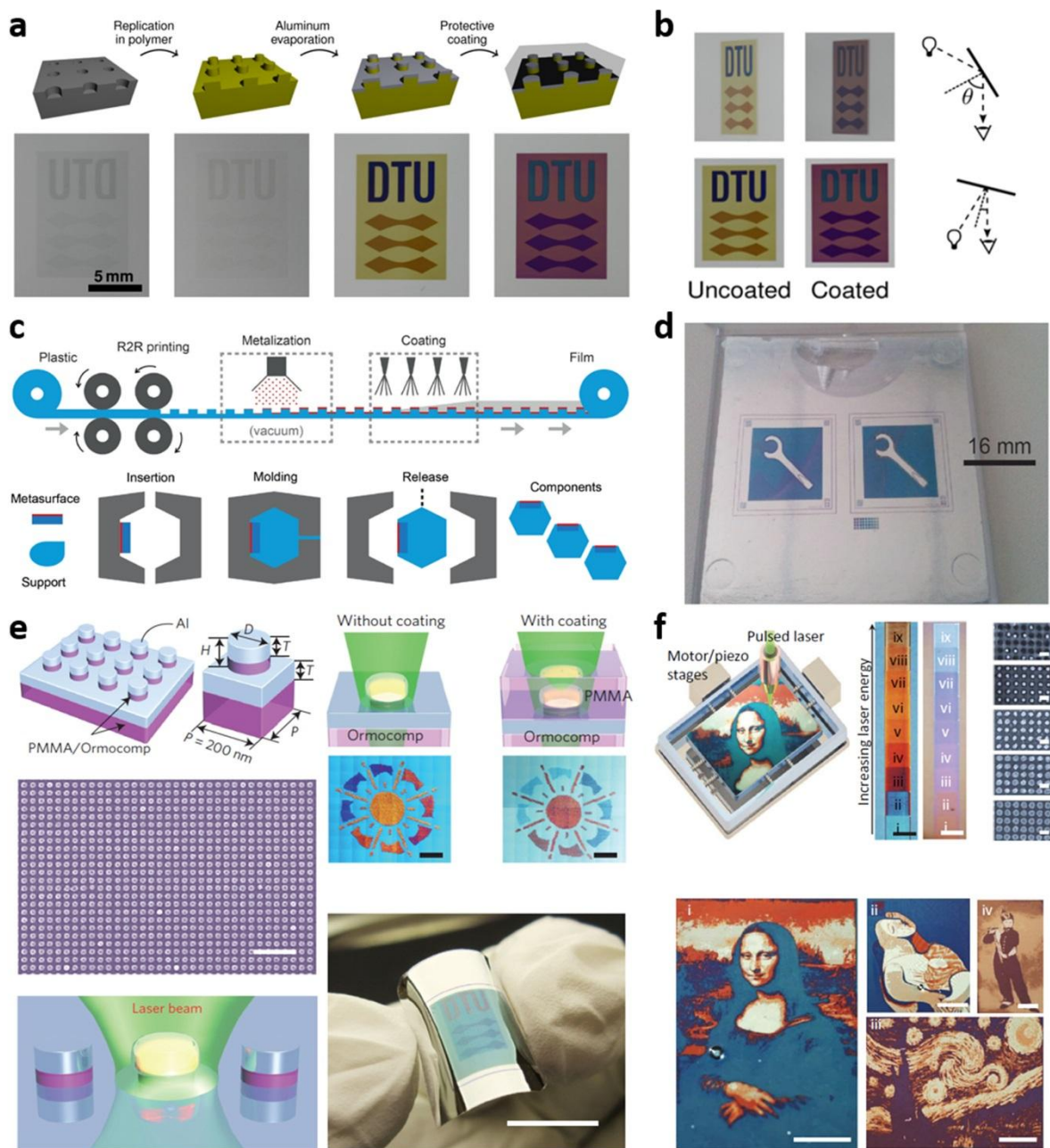


Figure 6. Top-down based large-area color printing techniques. (a) Flow chart for polymer replication. Hole-shaped master mold is used to extrude polymer pillar arrays using hot embossing method. After that, Al and protective layers are coated. (b) Pictures of printed metasurfaces with different viewing angles.¹⁵³ (c) Schematic for roll-to-roll printing (upper) and film-inserted molding process (lower). (d) Picture of fabricated large-area metasurfaces through film insert molding process.¹⁵⁴ (e) Schematic for plasmonic laser printing and corresponding fabricated colorful images. Using polymer replication method, arrays of nanopillars are fabricated, and further exposed to pulsed laser to tune their morphology and realize colorful images. (f) Schematic for resonant laser printing using dielectrics. Germanium (Ge) is used to make colors.^{157,158}

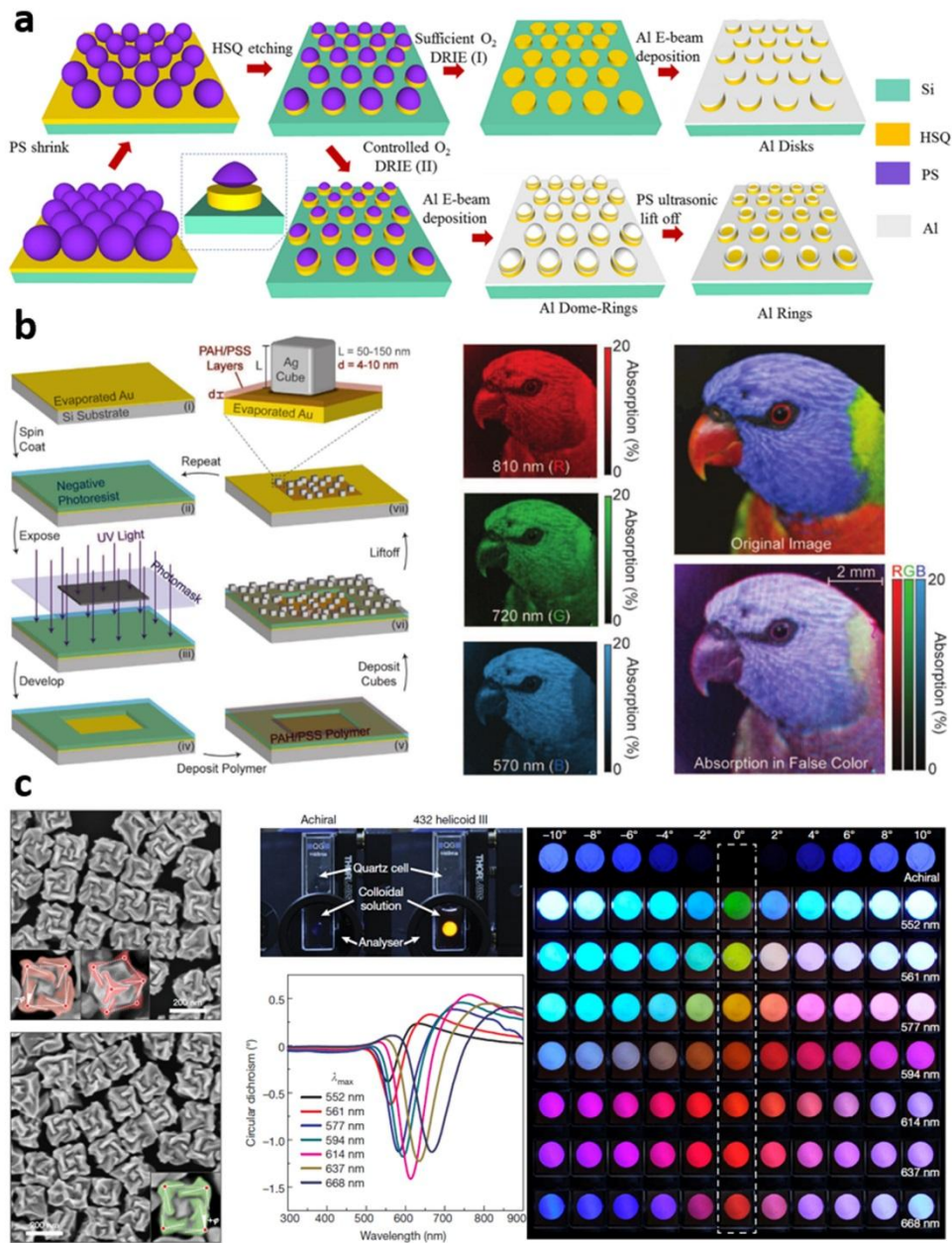


Figure 7. Bottom-up based large-area color printing techniques. (a) Process schematic using self-assembled colloids. Depending on etching and film deposition process, different geometries can be realized such as disks, dome-rings and rings.¹⁶¹ (b) Schematic for hybrid color printing techniques using colloidal nanoparticles and UV photolithography. Ag cube, spacing layer and bottom Au layer form MIM configurations. Depending on the size of cube and spacing layer thickness, absorbance spectrum will vary. Right images show reconstructed absorption images.¹⁶³ (c) Self-assembled chiral plasmonic particles with different handedness. Chiral particles can rotate visible electric field and thereby modulate the transmitted colors.¹⁶⁵

Outlook and future directions

Metasurfaces for display applications have rapidly advanced in the last decade. Development of nano-scale fabrication technology gives opportunity to realize sub-wavelength nanostructures with dimension suitable to address applications at visible frequencies. However, high cost of top-down approaches such as EBL, focused ion beam milling (FIB) hindered practical application of the metasurfaces. Due to the extremely low writing speed of EBL compared with photolithography, the feasible size of conventionally demonstrated metasurface holograms and color printing does not exceed 1 mm^2 . However, the recent advancements of large-scale manufacturing open new fabrication perspectives, and further stimulate a variety of research interest, in particular towards real-life applications of metasurfaces.¹⁵³⁻¹⁶⁵

Several key challenges have still to be addressed in both hologram and color printing approaches, *i.e.* low-loss material (high efficiency), dynamic/tunable mechanism and low fabrication cost. Low-loss dielectric materials like TiO_2 have drastically increased the efficiency of the metasurface at visible wavelengths but it needs atomic layer deposition process for a long time, which is usually challenging.^{16,17,58} Silicon-based metasurfaces benefit from well-established fabrication processes but their diffraction efficiency is currently not sufficient for the practical uses.^{55,77} Therefore, new materials or approaches are highly required to solve the dilemma of fabrication compatibility and diffraction efficiency. **The other challenge is unit cell controllability.** Many tunable mechanisms of metasurfaces have been developed to dynamically change the optical functionalities; nevertheless, it is still challenging to independently control individual unit cell of the metasurface, simply because the unit cells are too small to be individually addressed with electrical signals.^{166,167} In metasurface colorations, LC technology has been combined with plasmonic metasurfaces,¹⁶⁸ yet with all-dielectric structure, which may show highly bright and distinct tunable color spectra.^{169,170} Accordingly, there are still rooms for improvement of dynamic/tunable mechanism in the metasurfaces, which many of the outstanding studies are in great demand now.

So far, the functionality of metasurfaces towards reflective display has been studied in perspective of phase tuning and amplitude tuning, individually. The multi-functionality to manipulate both amplitude and phase distribution just began to be explored with the metasurface hologram platform with complicated geometrical design.¹⁷¹ By utilizing this technology the real 3D image which is exactly same as the object light may be realized with the metasurface hologram platform. As an alternative to manipulating amplitude and phase simultaneously, stereoscopic techniques can be adopted to generate 3D images. The 3D colorful image generation was demonstrated with polarization-dependence response of plasmonic structure, which employs overlaying two images under different polarization state orthogonal to each other via the microscope eyepieces.¹¹⁸ On the bounce, those multi-functional metasurfaces towards stereoscopic display can be highlighted as the following research topic.

The realization of metasurfaces on flexible and conformable substrates open new design perspectives for the realization of unexpected holographic images from various type of surfaces and geometries, as presented in Figure 8. For user-specified incident, transmitted, and reflected fields and a given surface geometry represented by the conformal coordinate system (u,v,n) , one can determine the required surface optical response to project a desired holographic image.^{173, 174} Various flexible metasurface components have been reported in particular Burch et al. have demonstrated that the shape of the interface can determine the properties of the far-field image, including its state of polarization. The focusing properties of metalenses is also affected by the geometry. The possibility of addressing light on arbitrary geometry will have important impact for the design of augmented reality displays. Plasmonic interfaces can also be combined with polymer thin films to realize new flexible and colorful electronic papers, providing fast response time and ultralow power consumption.

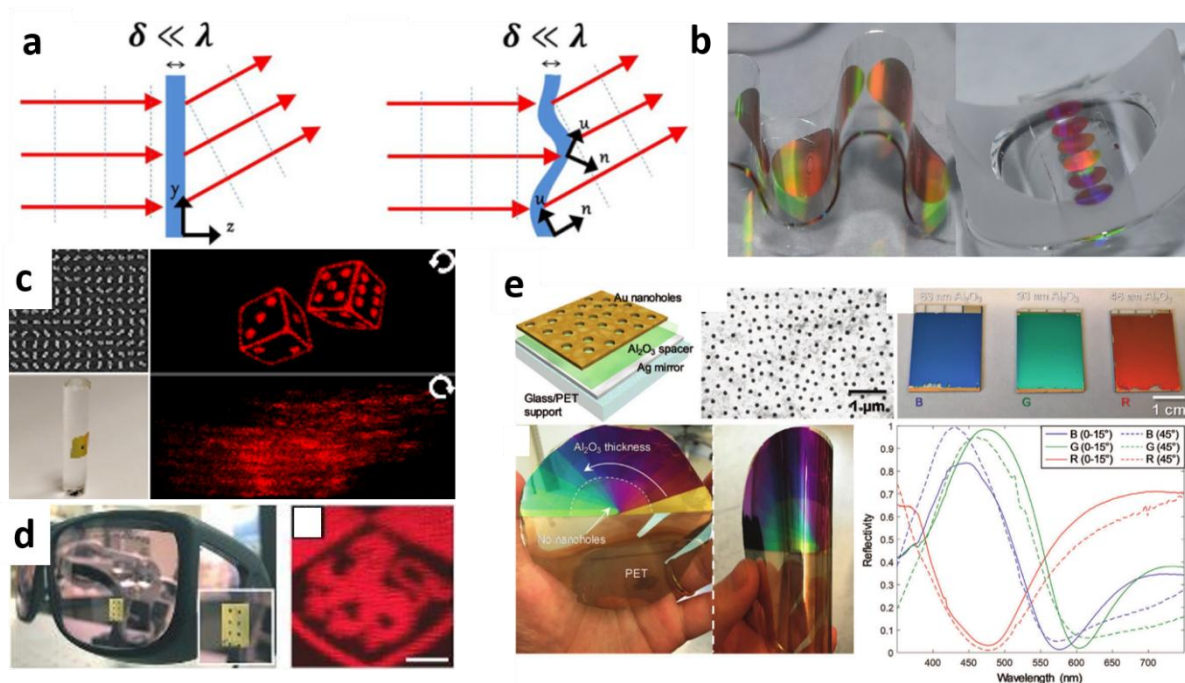


Figure 8. a- The realization of planar (left) or conformal (right) metasurfaces requires adapted modelling tools that can account for the effect of the physical distortion. Conformal boundary optics, a theoretical description of conformal boundary conditions, helps investigating reflection and refraction arising at the surface of arbitrarily-shaped objects . b- Infrared metalenses made on flexible substrates. c- Holographic metasurfaces designed for curved substrates can have different response according to both polarization and surface topology. d- Multiplexed holographic metasurfaces have been conformed to a pair of safety glasses. The inset is a close up of the metasurface and on the right the experimentally obtained image. e- Nano-holes gold plasmonic metasurfaces made on flexible substrate to control the reflection of RGB visible light.

Furthermore, device integrability will further expand optical metasurface based display applications.

For instance, company named e-skin Displays were launched and they designed the dynamic plasmonic nanostructure combined with LC, showing compatibility with flexible polyethylene terephthalate (PET) substrate and roll-to-roll nano-imprint lithography.^{138,139} Also, CMOS image sensors have been realized with plasmonic and dielectric nanohole design.^{94,106,107,172} The extremely thin perforated single-layer not only can be great alternative of conventional on-chip filters, but also be capable of microlenses on top of image sensor pixels. Besides, the subwavelength nanostructures of the metasurfaces afford anti-counterfeiting, cryptography, and optical data encryption. The versatile ways has been explored such as polarization multiplexing encryption,^{125,160} hydrogenation/dehydrogenation^{145,146} and can be realized by temperature-dependent optical response of phase-change materials.¹⁵⁰ With the above plethora of research efforts, optical metasurfaces would spread through in our life sooner or later.

Author Information

Corresponding Author

*E-mail: jsrho@postech.ac.kr

Notes

The authors have no competing financial interest.

Acknowledgements

This work is financially supported by the LGD-SNU Incubation program funded by LG Display and the National Research Foundation (NRF) grants (NRF-2015R1A5A1037668, NRF-2017R1E1A1A03070501, CAMM-2014M3A6B3063708, NRF-2017K1A3A1A21011645) funded by the Ministry of Science and ICT (MSIT), Republic of Korea. I.K. acknowledges the Global Ph.D. fellowship NRF-2016H1A2A1906519) funded by the NRF-MSIT, Republic of Korea. J.J. acknowledges a fellowship from Hyundai Motor Chung Mong-Koo Foundation. PG acknowledges financial support from the European Union's Horizon 2020 under the European Research Council

(ERC) grant agreement No. 639109 (project Flatlight). We also acknowledge financial support from the PHC STAR project (N° 38798RC)

References

- (1) Pendry, J. B. Negative Refraction Makes a Perfect Lens. *Phys. Rev. Lett.* **2000**, *85*, 3966
- (2) Shelby, R. A.; Smith, D. R.; Schultz, S. Experimental Verification of a Negative Index of Refraction. *Science* **2001**, *292*, 77-79
- (3) Fang, N.; Lee, H.; Sun, C.; Zhang, X. Sub-Diffraction-Limited Optical Imaging with a Silver Superlens. *Science* **2005**, *308*, 534-537
- (4) Liu, Z.; Lee, H.; Xiong, Y.; Sun, C.; Zhang, X. Far-Field Hyperlens Magnifying Sub-Diffraction-Limited Objects. *Science* **2007**, *315*, 1686
- (5) Rho, J.; Ye, Z.; Xiaobo, Y.; Liu, Z.; Choi, H.; Bartal, G.; Zhang, X. Spherical Hyperlens for Two-dimensional Sub-diffractive Imaging at Visible Frequencies. *Nat. Commun.* **2010**, *1*, 143
- (6) Cai, W.; Chettiar, U. K.; Kildishev, A. V.; Shalaev, V. M. Optical Cloaking with Metamaterials. *Nat. Photon.* **2007**, *1*, 224-227
- (7) Valentine, J.; Li, J.; Zentgraf, T.; Bartal, G.; Zhang, X. An Optical Cloak Made of Dielectrics. *Nat. Mater.* **2009**, *8*, 568-571
- (8) Ni, X.; Wong, Z. J.; Mrejen, M.; Wang, Y.; Zhang, X. An Ultrathin Invisibility Skin Cloak for Visible Light. *Science* **2015**, *349*, 1310-1314
- (9) Aydin, K.; Ferry, V. E.; Briggs, R. M.; Atwater, H. A. Broadband Polarization-independent Resonant Light Absorption Using Ultrathin Plasmonic Super Absorbers. *Nat. Commun.* **2011**, *2*, 517
- (10) Cui, Y.; Fung, K. H.; Xu, J.; Ma, H.; Jin, Y.; He, S.; Fang, N. X.; Ultrabroadband Light Absorption by a Sawtooth Anisotropic Metamaterial Slab. *Nano Lett.* **2012**, *12*, 1443-1447
- (11) Raman, A. P.; Anoma, M. A.; Zhu, L. Rephaeli, E.; Fan, S. Passive Radiative Cooling Below Ambient Air Temperature Under Direct Sunlight. *Nature* **2014**, *515*, 540-544
- (12) Feng, L.; Xu, Y.-L.; Fegadolli, W. S.; Lu, M.-H.; Oliveira, J. E. B.; Almeida, V. R.; Chen, Y.-F.; Scherer, A. Experimental Demonstration of a Unidirectional Reflectionless Parity-time Metamaterials at Optical Frequencies. *Nat. Mater.* **2013**, *12*, 108-113
- (13) Wong, Z. J.; Xu, Y.-L.; Kim, J.; O'Brien, K.; Wang, Y.; Feng, L.; Zhang, X. Lasing and Anti-lasing in A Single Cavity. *Nat. Photon.* **2016**, *10*, 796-801
- (14) Yu, N.; Capasso, F. Flat Optics with Designer Metasurfaces. *Nat. Mater.* **2014**, *13*, 139-150
- (15) Meinzer, N.; Barnes, W. L.; Hopper, I. R. Plasmonic Meta-atoms and Metasurfaces. *Nat. Photon.* **2014**, *8*, 889-898

- (16) Khorasaninejad, M.; Chen, W. T.; Devlin, R. C.; Oh, J.; Zhu, A. Y.; Capasso, F. Metalenses at Visible Wavelengths: Diffraction-limited Focusing and Subwavelength Resolution Imaging. *Science* **2016**, *352*, 1190-1194
- (17) Chen, W. T., Zhu, A. Y.; Sanjeev, V.; Khorasaninejad, M.; Shi, Z.; Lee, E.; Capasso, F. A Broadband Achromatic Metalens for Focusing and Imaging in The Visible. *Nat. Nanotechnol.* **2018**, *13*, 220-226
- (18) Wang, S.; Wu, P. C.; Su, V.-C.; Lai, Y.-C.; Chen, M.-K.; Kuo, H. Y.; Chen, B. H.; Chen, Y. H.; Huang, T.-T.; Wang, J.-H.; Lin, R.-M.; Kuan, C.-H.; Li, T.; Wang, Z.; Zhu, S.; Tsai, D. P. A Broadband Achromatic Metalens in The Visible. *Nat. Nanotechnol.* **2018**, *13*, 227-232
- (19) Jang, C.; Bang, K.; Moon, S.; Kim, J.; Lee, S.; Lee, B. Retinal 3D: Augmented Reality Near-Eye Display Via Pupil-Tracked Light Field Projection on Retina. *ACM Trans. Graph.* **2017**, *36*, 190
- (20) Gabor, D. A New Microscopic Principle. *Nature* **1948**, *161*, 777.
- (21) Blanche, P.-A.; Bablumian, A.; Voorakaranam, R.; Christenson, C.; Lin, W.; Gu, T.; Flores, D.; Wang, P.; Hsieh, W.-Y.; Kathaperumal, M.; Rachwal, B.; Siddiqui, O.; Thomas, J.; Norwood, R. A.; Yamamoto, M.; Peyghambarian, N. Holographic Three-Dimensional Telepresence Using Large-Area Photorefractive Polymer. *Nature* **2010**, *468*, 80–83.
- (22) Hao, C.; Nie, Z.; Ye, H.; Li, H.; Luo, Y.; Feng, R.; Yu, X.; Wen, F.; Zhang, Y.; Yu, C.; Teng, J.; Luk'yanchuk, B.; Qiu, C.-W. Three-Dimensional Supercritical Resolved Light-Induced Magnetic Holography. *Sci. Adv.* **2017**, *3*, e1701398.
- (23) Poon, T.-C.; Liu, J.-P. *Introduction to Modern Digital Holography: With MATLAB*; Cambridge University Press: New York, 2014.
- (24) Leith, E. N.; Upatnieks, J. Reconstructed Wavefronts and Communication Theory. *J. Opt. Soc. Am.* **1962**, *52*, 1123.
- (25) Lesem, L. B.; Hirsch, P. M.; Jordan, J. A. Scientific Applications: Computer Synthesis of Holograms for 3-D Display. *Commun. ACM* **1968**, *11*, 661–674.
- (26) Gerchberg, R. W.; Saxton, W. O. A Practical Algorithm for the Determination of the Phase from Image and Diffraction Plane Pictures. *Optik* **1972**, *35*, 237–246.
- (27) Dammann, H.; Görtler, K. High-Efficiency in-Line Multiple Imaging by Means of Multiple Phase Holograms. *Opt. Commun.* **1971**, *3*, 312–315.
- (28) Shen, F.; Wang, A. Fast-Fourier-Transform Based Numerical Integration Method for the Rayleigh-Sommerfeld Diffraction Formula. *Appl. Opt.* **2006**, *45*, 1102.

- (29) Walther, B.; Helgert, C.; Rockstuhl, C.; Pertsch, T. Diffractive Optical Elements Based on Plasmonic Metamaterials. *Appl. Phys. Lett.* **2011**, *98*, 191101.
- (30) Walther, B.; Helgert, C.; Rockstuhl, C.; Setzpfandt, F.; Eilenberger, F.; Kley, E.-B.; Lederer, F.; Tünnermann, A.; Pertsch, T. Spatial and Spectral Light Shaping with Metamaterials. *Adv. Mater.* **2012**, *24*, 6300–6304.
- (31) Larouche, S.; Tsai, Y.-J.; Tyler, T.; Jokerst, N. M.; Smith, D. R. Infrared Metamaterial Phase Holograms. *Nat. Mater.* **2012**, *11*, 450–454.
- (32) Kuester, E. F.; Mohamed, M. A.; Piket-May, M.; Holloway, C. L. Averaged Transition Conditions for Electromagnetic Fields at a Metafilm. *IEEE Trans. Antennas Propag.* **2003**, *51*, 2641–2651.
- (33) Holloway, C. L.; Dienstfrey, A.; Kuester, E. F.; O’Hara, J. F.; Azad, A. K.; Taylor, A. J. A Discussion on the Interpretation and Characterization of Metafilms/Metasurfaces: The Two-Dimensional Equivalent of Metamaterials. *Metamaterials* **2009**, *3*, 100–112.
- (34) Holloway, C. L.; Kuester, E. F.; Dienstfrey, A. Characterizing Metasurfaces/Metafilms: The Connection Between Surface Susceptibilities and Effective Material Properties. *IEEE Antennas Wirel. Propag. Lett.* **2011**, *10*, 1507–1511.
- (35) Holloway, C. L.; Love, D. C.; Kuester, E. F.; Gordon, J. A.; Hill, D. A. Use of Generalized Sheet Transition Conditions to Model Guided Waves on Metasurfaces/Metafilms. *IEEE Trans. Antennas Propag.* **2012**, *60*, 5173–5186.
- (36) Yu, N.; Capasso, F. Flat Optics with Designer Metasurfaces. *Nat. Mater.* **2014**, *13*, 139–150.
- (37) Zhang, L.; Mei, S.; Huang, K.; Qiu, C.-W. Advances in Full Control of Electromagnetic Waves with Metasurfaces. *Adv. Opt. Mater.* **2016**, *4*, 818–833.
- (38) Genevet, P.; Capasso, F.; Aieta, F.; Khorasaninejad, M.; Devlin, R. Recent Advances in Planar Optics: From Plasmonic to Dielectric Metasurfaces. *Optica* **2017**, *4*, 139.
- (39) Wan, W.; Gao, J.; Yang, X. Metasurface Holograms for Holographic Imaging. *Adv. Opt. Mater.* **2017**, *5*, 1700541.
- (40) Kock, W. E. Metallic Delay Lenses. *Bell Syst. Tech. J.* **1948**, *27*, 58–82.
- (41) Stork, W.; Streibl, N.; Haidner, H.; Kipfer, P. Artificial Distributed-Index Media Fabricated by Zero-Order Gratings. *Opt. Lett.* **1991**, *16*, 1921–1923.

- (42) Farn, M. W. Binary Gratings with Increased Efficiency. *Appl. Opt.* **1992**, *31*, 4453–4458.
- (43) Lalanne, P.; Astilean, S.; Chavel, P.; Cambriil, E.; Launois, H. Blazed Binary Subwavelength Gratings with Efficiencies Larger than Those of Conventional Échelette Gratings. *Opt. Express* **1998**, *23*, 1081.
- (44) Yu, N.; Genevet, P.; Kats, M. A.; Aieta, F.; Tetienne, J.-P.; Capasso, F.; Gaburro, Z. Light Propagation with Phase Discontinuities: Generalized Laws of Reflection and Refraction. *Science* **2011**, *334*, 333–337.
- (45) Ni, X.; Kildishev, A. V.; Shalaev, V. M. Metasurface Holograms for Visible Light. *Nat. Commun.* **2013**, *4*, 2807.
- (46) Bomzon, Z.; Kleiner, V.; Hasman, E. Pancharatnam–Berry Phase in Space-Variant Polarization-State Manipulations with Subwavelength Gratings. *Opt. Express* **2001**, *26*, 1424.
- (47) Huang, L.; Chen, X.; Mühlenbernd, H.; Li, G.; Bai, B.; Tan, Q.; Jin, G.; Zentgraf, T.; Zhang, S. Dispersionless Phase Discontinuities for Controlling Light Propagation. *Nano Lett.* **2012**, *12*, 5750–5755.
- (48) Huang, L.; Chen, X.; Mühlenbernd, H.; Zhang, H.; Chen, S.; Bai, B.; Tan, Q.; Jin, G.; Cheah, K.-W.; Qiu, C.-W.; Li, J. Zentgraf, T.; Zhang, S. Three-Dimensional Optical Holography Using a Plasmonic Metasurface. *Nat. Commun.* **2013**, *4*, 2808.
- (49) Yifat, Y.; Eitan, M.; Iluz, Z.; Hanein, Y.; Boag, A.; Scheuer, J. Highly Efficient and Broadband Wide-Angle Holography Using Patch-Dipole Nanoantenna Reflectarrays. *Nano Lett.* **2014**, *14*, 2485–2490.
- (50) Zheng, G.; Mühlenbernd, H.; Kenney, M.; Li, G.; Zentgraf, T.; Zhang, S. Metasurface Holograms Reaching 80% Efficiency. *Nat. Nanotech.* **2015**, *10*, 308–312.
- (51) Wen, D.; Yue, F.; Li, G.; Zheng, G.; Chan, K.; Chen, S.; Chen, M.; Li, K. F.; Wong, P. W. H.; Cheah, K. W.; Pun, E. Y. B.; Zhang, S.; Chen, X. Helicity Multiplexed Broadband Metasurface Holograms. *Nat. Commun.* **2015**, *6*, 8241.
- (52) Staude, I.; Miroshnichenko, A. E.; Decker, M.; Fofang, N. T.; Liu, S.; Gonzales, E.; Dominguez, J.; Luk, T. S.; Neshev, D. N.; Brener, I.; Kivshar, Y. Tailoring Directional Scattering through Magnetic and Electric Resonances in Subwavelength Silicon Nanodisks. *ACS Nano* **2013**, *7*, 7824–7832.
- (53) Staude, I.; Schilling, J. Metamaterial-Inspired Silicon Nanophotonics. *Nat. Photon.* **2017**, *11*, 274–284.

- (54) Arbabi, A.; Horie, Y.; Bagheri, M.; Faraon, A. Dielectric Metasurfaces for Complete Control of Phase and Polarization with Subwavelength Spatial Resolution and High Transmission. *Nat. Nanotech.* **2015**, *10*, 937–943.
- (55) Huang, K.; Dong, Z.; Mei, S.; Zhang, L.; Liu, Y.; Liu, H.; Zhu, H.; Teng, J.; Luk'yanchuk, B.; Yang, J. K. W.; Qiu, C.-W. Silicon Multi-Meta-Holograms for the Broadband Visible Light: Silicon Multi-Meta-Holograms for the Broadband Visible Light. *Laser Photonics Rev.* **2016**, *10*, 500–509.
- (56) Zhan, A.; Colburn, S.; Trivedi, R.; Fryett, T. K.; Dodson, C. M.; Majumdar, A. Low-Contrast Dielectric Metasurface Optics. *ACS Photonics* **2016**, *3*, 209–214.
- (57) Wang, S.; Wu, P. C.; Su, V.-C.; Lai, Y.-C.; Chen, M.-K.; Kuo, H. Y.; Chen, B. H.; Chen, Y. H.; Huang, T.-T.; Wang, J.-H.; Lin, R.-M.; Kuan, C.-H.; Li, T.; Wang, Z.; Zhu, S.; Tsai, D. P. A Broadband Achromatic Metalens in the Visible. *Nat. Nanotech.* **2018**, *13*, 227–232.
- (58) Devlin, R. C.; Khorasaninejad, M.; Chen, W. T.; Oh, J.; Capasso, F. Broadband High-Efficiency Dielectric Metasurfaces for the Visible Spectrum. *Proc. Natl. Acad. Sci. U.S.A.* **2016**, *113*, 10473–10478.
- (59) Montelongo, Y.; Tenorio-Pearl, J. O.; Williams, C.; Zhang, S.; Milne, W. I.; Wilkinson, T. D. Plasmonic Nanoparticle Scattering for Color Holograms. *Proc. Natl. Acad. Sci. U.S.A.* **2014**, *111*, 12679–12683.
- (60) Huang, Y.-W.; Chen, W. T.; Tsai, W.-Y.; Wu, P. C.; Wang, C.-M.; Sun, G.; Tsai, D. P. Aluminum Plasmonic Multicolor Meta-Hologram. *Nano Lett.* **2015**, *15*, 3122–3127.
- (61) Li, X.; Chen, L.; Li, Y.; Zhang, X.; Pu, M.; Zhao, Z.; Ma, X.; Wang, Y.; Hong, M.; Luo, X. Multicolor 3D Meta-Holography by Broadband Plasmonic Modulation. *Sci. Adv.* **2016**, *2*, e1601102.
- (62) Wan, W.; Gao, J.; Yang, X. Full-Color Plasmonic Metasurface Holograms. *ACS Nano* **2016**, *10*, 10671–10680.
- (63) Wang, B.; Dong, F.; Li, Q.-T.; Yang, D.; Sun, C.; Chen, J.; Song, Z.; Xu, L.; Chu, W.; Xiao, Y.-F.; Gong, Q.; Li, Y. Visible-Frequency Dielectric Metasurfaces for Multiwavelength Achromatic and Highly Dispersive Holograms. *Nano Lett.* **2016**, *16*, 5235–5240.
- (64) Wang, B.; Dong, F.; Yang, D.; Song, Z.; Xu, L.; Chu, W.; Gong, Q.; Li, Y. Polarization-Controlled Color-Tunable Holograms with Dielectric Metasurfaces. *Optica* **2017**, *4*, 1368.
- (65) Chen, W. T.; Yang, K.-Y.; Wang, C.-M.; Huang, Y.-W.; Sun, G.; Chiang, I.-D.; Liao, C. Y.; Hsu, W.-L.; Lin, H. T.; Sun, S.; Zhou, L.; Liu, A. Q.; Tsai, D. P. High-Efficiency Broadband Meta-Hologram with Polarization-Controlled Dual Images. *Nano Lett.* **2014**, *14*, 225–230.

- (66) Montelongo, Y.; Tenorio-Pearl, J. O.; Milne, W. I.; Wilkinson, T. D. Polarization Switchable Diffraction Based on Subwavelength Plasmonic Nanoantennas. *Nano Lett.* **2014**, *14*, 294–298.
- (67) Huang, L.; Mühlenbernd, H.; Li, X.; Song, X.; Bai, B.; Wang, Y.; Zentgraf, T. Broadband Hybrid Holographic Multiplexing with Geometric Metasurfaces. *Adv. Mater.* **2015**, *27*, 6444–6449.
- (68) Balthasar Mueller, J. P.; Rubin, N. A.; Devlin, R. C.; Groever, B.; Capasso, F. Metasurface Polarization Optics: Independent Phase Control of Arbitrary Orthogonal States of Polarization. *Phys. Rev. Lett.* **2017**, *118*, 113901.
- (69) Khorasaninejad, M.; Ambrosio, A.; Kanhaiya, P.; Capasso, F. Broadband and Chiral Binary Dielectric Meta-Holograms. *Sci. Adv.* **2016**, *2*, e1501258.
- (70) Kamali, S. M.; Arbabi, E.; Arbabi, A.; Horie, Y.; Faraji-Dana, M.; Faraon, A. Angle-Multiplexed Metasurfaces: Encoding Independent Wavefronts in a Single Metasurface under Different Illumination Angles. *Phys. Rev. X* **2017**, *7*, 041056.
- (71) Li, G.; Zhang, S.; Zentgraf, T. Nonlinear Photonic Metasurfaces. *Nat. Rev. Mater.* **2017**, *2*, 17010.
- (72) Ye, W.; Zeuner, F.; Li, X.; Reineke, B.; He, S.; Qiu, C.-W.; Liu, J.; Wang, Y.; Zhang, S.; Zentgraf, T. Spin and Wavelength Multiplexed Nonlinear Metasurface Holography. *Nat. Commun.* **2016**, *7*, 11930.
- (73) Almeida, E.; Bitton, O.; Prior, Y. Nonlinear Metamaterials for Holography. *Nat. Commun.* **2016**, *7*, 12533.
- (74) Chong, K. E.; Wang, L.; Staude, I.; James, A. R.; Dominguez, J.; Liu, S.; Subramania, G. S.; Decker, M.; Neshev, D. N.; Brener, I.; Kivshar, Y. S. Efficient Polarization-Insensitive Complex Wavefront Control Using Huygens' Metasurfaces Based on Dielectric Resonant Meta-Atoms. *ACS Photonics* **2016**, *3*, 514–519.
- (75) Wang, L.; Kruk, S.; Tang, H.; Li, T.; Kravchenko, I.; Neshev, D. N.; Kivshar, Y. S. Grayscale Transparent Metasurface Holograms. *Optica* **2016**, *3*, 1504.
- (76) Zhao, W.; Jiang, H.; Liu, B.; Song, J.; Jiang, Y.; Tang, C.; Li, J. Dielectric Huygens' Metasurface for High-Efficiency Hologram Operating in Transmission Mode. *Sci. Rep.* **2016**, *6*, 30613.
- (77) Yoon, G.; Lee, D.; Nam, K. T.; Rho, J. Pragmatic Metasurface Hologram at Visible Wavelength: The Balance between Diffraction Efficiency and Fabrication Compatibility. *ACS Photonics* **2018**, 10.1021/acsp Photonics.7b01044.

- (78) Huang, K.; Liu, H.; Si, G.; Wang, Q.; Lin, J.; Teng, J. Photon-Nanosieve for Ultrabroadband and Large-Angle-of-View Holograms: Photon-Nanosieve for Ultrabroadband and Large-Angle-of-View Holograms. *Laser Photonics Rev.* **2017**, *11*, 1700025.
- (79) Xie, Z.; Lei, T.; Si, G.; Wang, X.; Lin, J.; Min, C.; Yuan, X. Meta-Holograms with Full Parameter Control of Wavefront over a 1000 Nm Bandwidth. *ACS Photonics* **2017**, *4*, 2158–2164.
- (80) Lee, G.-Y.; Yoon, G.; Lee, S.-Y.; Yun, H.; Cho, J.; Lee, K.; Kim, H.; Rho, J.; Lee, B. Complete Amplitude and Phase Control of Light Using Broadband Holographic Metasurfaces. *Nanoscale* **2018**, *10*, 4237–4245.
- (81) Li, Z.; Kim, I.; Zhang, L.; Mehmood, M. Q.; Anwar, M. S.; Saleem, M.; Lee, D.; Nam, K. T.; Zhang, S.; Luk'yanchuk, B.; Zhang, G.; Rho, J.; Qiu, C.-W. Dielectric Meta-Holograms Enabled with Dual Magnetic Resonances in Visible Light. *ACS Nano* **2017**, *11*, 9382–9389.
- (82) Liu, H.-C.; Yang, B.; Guo, Q.; Shi, J.; Guan, C.; Zheng, G.; Mühlenbernd, H.; Li, G.; Zentgraf, T.; Zhang, S. Single-Pixel Computational Ghost Imaging with Helicity-Dependent Metasurface Hologram. *Sci. Adv.* **2017**, *3*, e1701477.
- (83) Malek, S. C.; Ee, H.-S.; Agarwal, R. Strain Multiplexed Metasurface Holograms on a Stretchable Substrate. *Nano Lett.* **2017**, *17*, 3641–3645.
- (84) Heikenfeld, J.; Drzaic, P.; Yeo, J.-S.; Koch, T. A Critical Review of The Present and Future Prospects for electronic paper. *J. Soc. Inf. Display* **2011**, *19*, 129-156.
- (85) “iRex Takes On The Kindle”, *Forbes*, 2008-09-23.
- (86) Arsenault, A. C.; Puzzo, D. P.; Manners, I.; Ozin, G. A. Photonic-crystal Full-colour Displays. *Nat. Photon.* **2007**, *1*, 468-472.
- (87) Kim, H.; Ge, J.; Kim, J.; Choi, S.-E.; Lee, H.; Lee, H.; Park, W.; Yin, Y.; Kwon, S. Structural Colour Printing Using a Magnetically Tunable and Lithographically Fixable Photonic Crystal. *Nat. Photon.* **2009**, *3*, 534-540.
- (88) Shen, Y.; Rinnerbauer, V.; Wang, I.; Stelmakh, V.; Joannopoulos, J. D.; Soljačić, M. Structure Colors from Fano Resonances. *ACS Nano* **2015**, *2*, 27-32.
- (89) Lee, S. Y.; Choi, J.; Jeong, J.-R.; Shin, J. H.; Kim, S.-H. Magneto-responsive Photonic Microspheres with Structural Color Gradient. *Adv. Mater.* **2017**, *29*, 1605450.
- (90) Cho, S.; Shim, T.; Kim, J. H.; Kim, D. H.; Kim, S.-H. Selective Coloration of Melanin Nanospheres through Resonant Mie Scattering. *Adv. Mater.* **2017**, *29*, 1700256.
- (91) Xu, T.; Wu, Y.-K.; Luo, X.; Guo, L. J. Plasmonic Nanoresonators for High-resolution Colour Filtering and Spectral Imaging. *Nat. Commun.* **2010**, *1*, 59.

- (92) Duempelmann, L.; Casari, D.; Luu-Dinh, A.; Gallinet, B.; Novotny, L. Color Rendering Plasmonic Aluminum Substrates with Angular Symmetry Breaking. *ACS Nano* **2015**, *9*, 12383–12391.
- (93) Duempelmann, L.; Luu-Dinh, A.; Gallinet, B.; Novotny, L. Four-fold Color Filter Based on Plasmonic Phase Retarder. *ACS Photonics* **2016**, *3*, 190-196.
- (94) Horie, Y.; Han, S.; Lee, J.-Y.; Kim, J.; Kim, Y.; Arbabi, A.; Shin, C.; Shi, L.; Kamali, S. M.; Lee, H.-S.; Hwang, S.; Faraon, A. Visible Wavelength Color Filters Using Dielectric Subwavelength Gratings for Backside-Illuminated CMOS Image Sensor Technologies. *Nano Lett.* **2017**, *17*, 3159-3164.
- (95) Duempelmann, L.; Gallinet, B.; Novotny, L. Multispectral Imaging with Tunable Plasmonic Filters. *ACS Photonics* **2017**, *4*, 236–241.
- (96) Kats, M. A.; Blanchard, R.; Genevet, P.; Capasso, F. Nanometre Optical Coatings based on Strong Interference Effects in Highly Absorbing Media. *Nat. Mater.* **2013**, *12*, 20-24.
- (97) Chung, K.; Yu, S.; Heo, C.-J.; Shim, J. W.; Yang, S.-M.; Han, M. G.; Lee, H.-S.; Jin, Y.; Lee, S. Y.; Park, N.; Shin, J. H. Flexible, Angle-Independent, Structure Color Reflectors Inspired by Morpho Butterfly Wings. *Adv. Mater.* **2012**, *24*, 2375-2379.
- (98) Kristensen, A.; Yang, J. K. W.; Bozhevolnyi, S. I.; Link, S.; Nordlander, P.; Halas, N. J.; Mortensen, N. A. Plasmonic Colour Generation. *Nat. Rev. Mater.* **2016**, *2*, 16088.
- (99) Lee, T.; Jang, J.; Jeong, H.; Rho, J. Plasmonic- and Dielectric-Based Structural Coloring: From Fundamentals to Practical Applications. *Nano Convergence* **2018**, *5*, 1.
- (100) Kumar, K.; Duan, H.; Hegde, R. S.; Koh, S. C. W.; Wei, J. N.; Yang, J. K. W. Printing Colour at the Optical Diffraction Limit. *Nat. Nanotechnol.* **2012**, *7*, 557–561.
- (101) Ellenbogen, T.; Seo, K.; Crozier, K. B. Chromatic Plasmonic Polarizers for Active Visible Color Filtering and Polarimetry. *Nano Lett.* **2012**, *12*, 1026–1031.
- (102) Olson, J.; Manjavacas, A.; Liu, L.; Chang, W.-S.; Foerster, B.; King, N. S.; Knight, M. W.; Nordlander, P.; Halas, N. J.; Link, S. Vivid, Full-Color Aluminum Plasmonic Pixels. *Proc. Natl. Acad. Sci. U.S.A.* **2014**, *111*, 14348–14353.
- (103) James, T. D.; Mulvaney, P.; Roberts, A. The Plasmonic Pixel: Large Area, Wide Gamut Color Reproduction Using Aluminum Nanostructures. *Nano Lett.* **2016**, *16*, 3817–3823.
- (104) Lee, H.-S.; Yoon, Y.-T.; Lee, S.-S.; Kim, S.-H.; Lee, K.-D. Color Filter Based on a Subwavelength Patterned Metal Grating. *Opt. Express* **2007**, *15*, 15457–15463.
- (105) Chen, Q.; Cumming, D. R. S. High Transmission and Low Color Cross-Talk Plasmonic Color Filters Using Triangular-Lattice Hole Arrays in Aluminum Films. *Opt. Express* **2010**, *18*, 14056–14062.

- (106) Yokogawa, S.; Burgos, S. P.; Atwater, H. A. Plasmonic Color Filters for CMOS Image Sensor Applications. *Nano Lett.* **2012**, *12*, 4349–4354.
- (107) Burgos, S. P.; Yokogawa, S.; Atwater, H. A. Color Imaging via Nearest Neighbor Hole Coupling in Plasmonic Color Filters Integrated onto a Complementary Metal-Oxide Semiconductor Image Sensor. *ACS Nano* **2013**, *7*, 10038–10047.
- (108) Cheng, F.; Gao, J.; Luk, T. S.; Yang, X. Structural Color Printing based on Plasmonic Metasurfaces of Perfect Light Absorption. *Sci. Rep.* **2015**, *5*, 11045.
- (109) Yun, H.; Lee, S.-Y.; Hong, K.; Yeom, J.; Lee, B. Plasmonic Cavity-apertures as Dynamic Pixels for the Simultaneous Control of Colour and Intensity. *Nat. Commun.* **2015**, *6*, 7133.
- (110) Wang, W.; Rosenmann, D.; Czaplewski, D. A.; Yang, X.; Gao, J. Realizing Structural Color Generation with Aluminum Plasmonic V-groove Metasurfaces. *Opt. Express* **2017**, *25*, 20454–20465.
- (111) Li, Z.; Clark, A. W.; Cooper, J. M. Dual Color Plasmonic Pixels Create a Polarization Controlled Nano Color Palette. *ACS Nano* **2016**, *10*, 492–498.
- (112) Heydari, E.; Sperling, J. R.; Neale, S. L.; Clark, A. W. Plasmonic Color Filters as Dual-State Nanopixels for High-Density Microimage Encoding. *Adv. Funct. Mater.* **2017**, *27*, 1701866.
- (113) Xu, T.; Wu, Y.-K.; Luo, X.; Guo, L. J. Plasmonic Nanoresonators for High-Resolution Colour Filtering and Spectral Imaging. *Nat. Commun.* **2010**, *1*, 59.
- (114) Duempelmann, L.; Luu-Dinh, A.; Gallinet, B.; Novotny, L. Four-Fold Color Filter Based on Plasmonic Phase Retarder. *ACS Photonics* **2016**, *3*, 190–196.
- (115) Duempelmann, L.; Gallinet, B.; Novotny, L. Multispectral Imaging with Tunable Plasmonic Filters. *ACS Photonics* **2017**, *4*, 236–241.
- (116) Kumar, K.; Duan, H.; Hegde, R. S.; Koh, S. C. W.; Wei, J. N.; Yang, J. K. W. Printing Colour at the Optical Diffraction Limit. *Nat. Nanotechnol.* **2012**, *7*, 557–561.
- (117) Tan, S. J.; Zhang, L.; Zhu, D.; Goh, X. M.; Wang, Y. M.; Kumar, K.; Qiu, C. W.; Yang, J. K. W. Plasmonic Color Palettes for Photorealistic Printing with Aluminum Nanostructures. *Nano Lett.* **2014**, *14*, 4023–4029.
- (118) Goh, X. M.; Zheng, Y.; Tan, S. J.; Zhang, L.; Kumar, K.; Qiu, C.-W.; Yang, J. K. W. Three-Dimensional Plasmonic Stereoscopic Prints in Full Colour. *Nat. Commun.* **2014**, *5*, 6361.
- (119) Roberts, A. S.; Pors, A.; Albrechtsen, O.; Bozhevolnyi, S. I. Subwavelength Plasmonic Color Printing Protected for Ambient Use. *Nano Lett.* **2014**, *14*, 783–787.
- (120) Wang, H.; Wang, X.; Yan, C.; Zhao, H.; Zhang, J.; Santschi, C.; Martin, O. J. F. Full Color Generation Using Silver Tandem Nanodisks. *ACS Nano*, **2017**, *11*, 20454–20465.
- (121) Flauraud, V.; Reyes, M.; Paniagua-Domínguez, R.; Kuznetsov, A. I.; Brugger, J. Silicon Nanostructures for Bright Field Full Color Prints. *ACS Photonics* **2017**, *4*, 1913–1919.

- (122) Vashistha, V.; Vaidya, G.; Hegde, R. S.; Serebryannikov, A. E.; Bonod, N.; Krawczyk, M. All-Dielectric Metasurfaces Based on Cross-Shaped Resonators for Color Pixels with Extended Gamut. *ACS Photonics* **2017**, *4*, 1076-1082.
- (123) Dong, Z.; Ho, J.; Yu, Y. F.; Fu, Y. H.; Paniagua-Domínguez, R.; Wang, S.; Kuznetsov, A. I.; Yang, J. K. W. Printing Beyond sRGB Color Gamut by Mimicking Silicon Nanostructures in Free-Space. *Nano Lett.* **2017**, *17*, 7620-7628.
- (124) Nagasaki, Y.; Suzuki, M.; Hotta, I.; Takahara, J. Control of Si-Based All-Dielectric Printing Color through Oxidation. *ACS Photonics*. **2018**, 10.1021/acsp Photonics.7b01467.
- (125) Nagasaki, Y.; Suzuki, M.; Takahara, J. All-Dielectric Dual-Color Pixel with Subwavelength Resolution. *Nano Lett.* **2017**, *17*, 7500–7506.
- (126) Wood, T.; Naffouti, M.; Berthelot, J.; David, T.; Claude, J.-B.; Métayer, L.; Delobbe, A.; Favre, L.; Ronda, A.; Berbezier, I.; Bonod, N.; Abbarchi, M. All-Dielectric Color Filters Using SiGe-Based Mie Resonator Arrays. *ACS Photonics* **2017**, *4*, 873–883.
- (127) Park, C.-S.; Shrestha, V. R.; Yue, W.; Gao, S.; Lee, S.-S.; Kim, E.-S.; Choi, D.-Y. Structural Color Filters Enabled by a Dielectric Metasurface Incorporating Hydrogenated Amorphous Silicon Nanodisks. *Sci. Rep.* **2017**, *7*, 2556.
- (128) Sun, S.; Zhou, Z.; Zhang, C.; Gao, Y.; Duan, Z.; Xiao, S.; Song, Q. All-Dielectric Full-Color Printing with TiO₂ Metasurfaces. *ACS Nano* **2017**, *11*, 4445-4452.
- (129) Sun, S.; Yang, W.; Zhang, C.; Jing, J.; Gao, Y.; Yu, X.; Song, Q.; Xiao, S. Real-Time Tunable Colors from Microfluidic Reconfigurable All-Dielectric Metasurfaces. *ACS Nano* **2018**, *12*, 2151-2159.
- (130) Kerker, M.; Wang, D.-S.; Giles, C. L. Electromagnetic Scattering by Magnetic Spheres. *J. Opt. Soc. Am.* **1983**, *73*, 765–767.
- (131) Geffrin, J. M.; García-Cámara, B.; Gómez-Medina, R.; Albella, P.; Froufe-Pérez, L. S.; Eyraud, C.; Litman, A.; Vaillon, R.; González, F.; Nieto-Vesperinas, M.; Sáenz, J. J.; Moreno, F. Magnetic and Electric Coherence in Forward- and Back-Scattered Electromagnetic Waves by a Single Dielectric Subwavelength Sphere. *Nat. Commun.* **2012**, *3*, 2167.
- (132) Fu, Y. H.; Kuznetsov, A. I.; Miroshnichenko, A. E.; Yu, Y. F.; Luk'yanchuk, B. Directional Visible Light Scattering by Silicon Nanoparticles. *Nat. Commun.* **2013**, *4*, 1527.
- (133) Paniagua-Domínguez, R.; Yu, Y. F.; Miroshnichenko, A. E.; Krivitsky, L. A.; Fu, Y. H.; Valuckas, V.; Gonzaga, L.; Toh, Y. T.; Kay, A. Y. S.; Luk'yanchuk, B.; Kuznetsov, A. I. Generalized Brewster Effect in Dielectric Metasurfaces. *Nat. Commun.* **2016**, *7*, 10362.
- (134) Shen, Y.; Rinnerbauer, V.; Wang, I.; Stelmakh, V.; Joannopoulos, J. D.; Soljačić, M. Structural Colors from Fano Resonances. *ACS Photonics* **2015**, *2*, 27–32.

- (135) Zhu, L.; Kapraun, J.; Ferrara, J.; Chang-Hasnain, C. J. Flexible Photonic Metastructures for Tunable Coloration. *Optica* **2015**, *2*, 255–258.
- (136) Gutruf, P.; Zou, C.; Withayachumnankul, W.; Bhaskaran, M.; Sriram, S.; Fumeaux, C. Mechanically Tunable Dielectric Resonator Metasurfaces at Visible Frequencies. *ACS Nano* **2016**, *10*, 133–141.
- (137) Tseng, M. L.; Yang, J.; Semmlinger, M.; Zhang, C.; Nordlander, P.; Halas, N. J. Two-Dimensional Active Tuning of an Aluminum Plasmonic Array for Full-Spectrum Response. *Nano Lett.* **2017**, *17*, 6034–6039.
- (138) Franklin, D.; Chen, Y.; Vazquez-Guardado, A.; Modak, S.; Boroumand, J.; Xu, D.; Wu, S.-T.; Chanda, D. Polarization-Independent Actively Tunable Colour Generation on Imprinted Plasmonic Surfaces. *Nat. Commun.* **2015**, *6*, 7337.
- (139) Franklin, D.; Frank, R.; Wu, S.-T.; Chanda, D. Actively Addressed Single Pixel Full-Colour Plasmonic Display. *Nat. Commun.* **2017**, *8*, 15209.
- (140) Olson, J.; Manjavacas, A.; Basu, T.; Huang, D.; Schlather, A. E.; Zheng, B.; Halas, N. J.; Nordlander, P.; Link, S. High Chromaticity Aluminum Plasmonic Pixels for Active Liquid Crystal Displays. *ACS Nano* **2016**, *10*, 1108–1117.
- (141) Richner, P.; Galliker, P.; Lendenmann, T.; Kress, S. J. P.; Kim, D. K.; Norris, D. J.; Poulikakos, D. Full-Spectrum Flexible Color Printing at the Diffraction Limit. *ACS Photonics* **2016**, *3*, 754–757.
- (142) Xiong, K.; Emilsson, G.; Maziz, A.; Yang, X.; Shao, L.; Jager, E. W. H.; Dahlin, A. B. Plasmonic Metasurfaces with Conjugated Polymers for Flexible Electronic Paper in Color. *Adv. Mater.* **2016**, *28*, 9956–9960.
- (143) Xiong, K.; Tordera, D.; Emilsson, G.; Olsson, O.; Linderhed, U.; Jonsson, M. P.; Dahlin, A. B. Switchable Plasmonic Metasurfaces with High Chromaticity Containing Only Abundant Metals. *Nano Lett.* **2017**, *17*, 7033–7039.
- (144) Xu, T.; Walter, E. C.; Agrawal, A.; Bohn, C.; Velmurugan, J.; Zhu, W.; Lezec, H. J.; Talin, A. A. High-Contrast and Fast Electrochromic Switching Enabled by Plasmonics. *Nat. Commun.* **2016**, *7*, 10479.
- (145) Duan, X.; Kamin, S.; Liu, N. Dynamic Plasmonic Colour Display. *Nat. Commun.* **2017**, *8*, 14606.
- (146) Chen, Y.; Duan, X.; Matuschek, M.; Zhou, Y.; Neubrech, F.; Duan, H.; Liu, N. Dynamic Color Displays Using Stepwise Cavity Resonators. *Nano Lett.* **2017**, *17*, 5555–5560.
- (147) Wang, G.; Chen, X.; Liu, S.; Wong, C.; Chu, S. Mechanical Chameleon through Dynamic Real-Time Plasmonic Tuning. *ACS Nano* **2016**, *10*, 1788–1794.

- (148) Yun, H.; Lee, S.-Y.; Hong, K.; Yeom, J.; Lee, B. Plasmonic Cavity-Apertures as Dynamic Pixels for the Simultaneous Control of Colour and Intensity. *Nat. Commun.* **2015**, *6*, 7133.
- (149) Yang, B.; Liu, W.; Li, Z.; Cheng, H.; Chen, S.; Tian, J. Polarization-Sensitive Structural Colors with Hue-and-Saturation Tuning Based on All-Dielectric Nanopixels. *Adv. Opt. Mater.* **2018**, *6*, 1701009.
- (150) Shu, F.-Z.; Yu, F.-F.; Peng, R.-W.; Zhu, Y.-Y.; Xiong, B.; Fan, R.-H.; Wang, Z.-H.; Liu, Y.; Wang, M. Dynamic Plasmonic Color Generation Based on Phase Transition of Vanadium Dioxide. *Adv. Opt. Mater.* **2018**, *6*, 1700939.
- (151) Park, C.-H.; Yoon, Y.-T.; Shrestha, V. R.; Park, C.-S.; Lee, S.-S.; Kim, E.-S. Electrically Tunable Color Filter Based on a Polarization-Tailored Nano-Photonic Dichroic Resonator Featuring an Asymmetric Subwavelength Grating. *Opt. Express* **2013**, *21*, 28783–28793.
- (152) Kats, M. A.; Blanchard, R.; Genevet, P.; Yang, Z.; Qazilbash, M. M.; Basov, D. N.; Ramanathan, S.; Capasso, F. Thermal Tuning of Mid-Infrared Plasmonic Antenna Arrays Using a Phase Change Materials. *Opt. Lett.* **2013**, *38*, 368-370
- (153) Clausen, J. S.; Højlund-Nielsen, E.; Christiansen, A. B.; Yazdi, S.; Grajower, M.; Taha, H.; Levy, U.; Kristensen, A.; Mortensen, N. A. Plasmonic Metasurfaces for Coloration of Plastic Consumer Products. *Nano Lett.* **2014**, *14*, 4499-4504.
- (154) Højlund-Nielsen, E; Clausen, J.; Mäkela, T.; Thamdrup, L. H.; Zalkovskij, M.; Nielsen, T.; Pira, N. L.; Ahopelto, J.; Mortensen, N. A.; Kristensen, A. Plasmonic Colors: Toward Mass Production of Metasurfaces. *Adv. Mater. Technol.* **2016**, *1*, 1600054.
- (155) Lu, B.-R.; Xu, C.; Liao, J.; Liu, J.; Chen, Y. High-Resolution Plasmonic Structural Colors from Nanohole Arrays with Bottom Metal Disks. *Opt. Lett.* **2016**, *41*, 1400–1403.
- (156) Do, Y. S.; Park, J. H.; Hwang, B. Y.; Lee, S.-M.; Ju, B.-K.; Choi, K. C. Plasmonic Color Filter and Its Fabrication for Large-Area Applications. *Adv. Opt. Mater* **2013**, *1*, 133–138.
- (157) Zhu, X.; Vannahme, C.; Højlund-Nielsen, E.; Mortensen, N. A.; Kristensen, A. Plasmonic Colour Laser Printing. *Nat. Nanotechnol.* **2015**, *11*, 325-329.
- (158) Zhu, X.; Yan, W.; Levy, U.; Mortensen, N. A.; Kristensen, A. Resonant Laser Printing of Structural Colors on High-Index Dielectric Metasurfaces. *Sci. Adv.* **2017**, *3*, e1602487.
- (159) Guay, J.-M.; Lesina, A. C.; Côté, G.; Charron, M.; Poitras, D.; Ramunno, L.; Berini, P.; Weck, A. Laser-Induced Plasmonic Colours on Metals. *Nat. Commun.* **2017**, *8*, 16095.
- (160) Xue, J.; Zhou, Z.-K.; Wei, Z.; Su, R.; Lai, J.; Li, J.; Li, C.; Zhang, T.; Wang, X.-H. Scalable, Full-Colour and Controllable Chromotropic Plasmonic Printing. *Nat. Commun.* **2015**, *6*, 8906.
- (161) Wang, L.; Ng, R. J. H.; Safari Dinachali, S.; Jalali, M.; Yu, Y.; Yang, J. K. W. Large Area Plasmonic Color Palettes with Expanded Gamut Using Colloidal Self-Assembly. *ACS Photonics* **2016**, *3*, 627–633.

- (162) Xiong, K.; Tordera, D.; Emilsson, G.; Olsson, O.; Linderhed, U.; Jonsson, M. P.; Dahlin, A. B. Switchable Plasmonic Metasurfaces with High Chromaticity Containing Only Abundant Metals. *Nano Lett.* **2017**, *17*, 7033–7039.
- (163) Stewart, J. W.; Akselrod, G. M.; Smith, D. R.; Mikkelsen, M. H. Toward Multispectral Imaging with Colloidal Metasurface Pixels. *Adv. Mater.* **2017**, *29*, 1602971.
- (164) Galinski, H.; Favraud, G.; Dong, H.; Gongora, J. S. T.; Favaro, G.; Döbeli, M.; Spolenak, R.; Fratolocci, A.; Capasso, F. Scalable, Ultra-Resistant Structural Colors Based on Network Metamaterials. *Light Sci. Appl.* **2017**, *6*, e16233.
- (165) Lee, H.; Ahn, H.-Y.; Mun, J.; Lee, Y. Y.; Kim, M.; Cho, N. H.; Chang, K.; Kim, W. S.; Rho, J.; Nam, K. T.; Amino-acid- and Peptide-directed Synthesis of Chiral Plasmonic Gold Particles. *Nature* **2018**, *556*, 360-365
- (166) Yao, Y.; Shankar, R.; Kats, M. A.; Song, Y.; Kong, J.; Loncar, M.; Capasso, F. Electrically Tunable Metasurface Perfect Absorbers for Ultrathin Mid-Infrared Optical Modulators. *Nano Lett.* **2014**, *14*, 6526–6532.
- (167) Zhu, Z.; Evans, P. G.; Haglund, R. F.; Valentine, J. G. Dynamically Reconfigurable Metadevice Employing Nanostructured Phase-Change Materials. *Nano Lett.* **2017**, *17*, 4881–4885.
- (168) Bartholomew, R.; Williams, C.; Khan, A.; Bowman, R.; Wilkinson, T. Plasmonic Nanohole Electrodes for Active Color Tunable Liquid Crystal Transmissive Pixels. *Opt. Lett.* **2017**, *42*, 2810–2813.
- (169) Komar, A.; Fang, Z.; Bohn, J.; Sautter, J.; Decker, M.; Miroshnichenko, A.; Pertsch, T.; Brener, I.; Kivshar, Y. S.; Staude, I.; Neshev, D. N. Electrically Tunable All-Dielectric Optical Metasurfaces Based on Liquid Crystals. *Appl. Phys. Lett.* **2017**, *110*, 071109.
- (170) Komar, A.; Paniagua-Domínguez, R.; Miroshnichenko, A.; Yu, Y. F.; Kivshar, Y. S.; Kuznetsov, A. I.; Neshev, D. Dynamic Beam Switching by Liquid Crystal Tunable Dielectric Metasurfaces. *ACS Photonics* **2018**, 10.1021/acsp Photonics.7b01343.
- (171) Zang, X.; Dong, F.; Yue, F.; Zhang, C.; Xu, L.; Song, Z.; Chen, M.; Chen, P.-Y.; Buller, G. S.; Zhu, Y.; Zhuang, S.; Chu, W.; Zhang, S.; Chen, X. Polarization Encoded Color Image Embedded in a Dielectric Metasurface. *Adv. Mater.* **2018**, 1707499.
- (172) Chen, Q.; Das, D.; Chitnis, D.; Walls, K.; Drysdale, T. D.; Collins, S.; Cumming, D. R. S. A CMOS Image Sensor Integrated with Plasmonic Colour Filters. *Plasmonics* **2012**, *7*, 695–699.
- (173) Teo, J. T. H.; Wong, L. J.; Molardi, C.; Genevet, P. Controlling electromagnetic fields at boundaries of arbitrary geometries. *Phys. Rev. A* **2016**, *94*, 023820
- (174) Wu, K.; Coquet, P.; Wang, Q. J.; Genevet, P. Modelling of Free-form Conformal Metasurfaces, accepted *Nat. Commun.* (2018)

